LISBOA
SCHOOL OF
ECONOMICS &
MANAGEMENT

MESTRADO

ACTUARIAL SCIENCE

TRABALHO FINAL DE MESTRADO

DISSERTAÇÃO

MODELING SOVEREIGN DEBT WITH LÉVY PROCESSES

GONÇALO ANDRÉ NUNES PEREIRA

OUTUBRO - 2014

LISBOA SCHOOL OF ECONOMICS & MANAGEMENT

SINCE 1911

MESTRADO EM

ACTUARIAL SCIENCE

TRABALHO FINAL DE MESTRADO

DISSERTAÇÃO

MODELING SOVEREIGN DEBT WITH LÉVY PROCESSES

GONÇALO ANDRÉ NUNES PEREIRA

ORIENTAÇÃO:

RAQUEL GASPAR
JOÃO GUERRA

OUTUBRO - 2014

Abstract

We propose to model the sovereign credit risk of five Euro area countries (Portugal, Ireland, Italy, Greece and Spain) under a first passage structural approach, replacing the classical geometric Brownian motion dynamics with a pure jump Lévy process. This framework caters for skewness, fat tails and instantaneous defaults, thus addressing some of the main drawbacks of the Black-Scholes model.

We compute the survival probability as the price of a discrete barrier option, using an option pricing method based on the approximation of the transition density as a Fourier-cosine series expansion. Assuming a deterministic recovery rate, we calibrate the Carr–Geman–Madan–Yor (CGMY) Lévy model to weekly Credit Default Swaps data and obtain the default probability term structure. By drawing on the representation of the Variance Gamma process (a particular instance of the CGMY model) as a time-changed Brownian motion, we accommodate dependency between sovereigns via a common time change. We then illustrate a possible multivariate calibration procedure and simulate the joint default distribution.

Keywords: Credit risk; Lévy processes; Sovereign debt; Credit Default Swaps; Default probability; Fourier-cosine expansion; Time-changed Brownian motion.

Resumo

Propomos modelizar o risco de crédito soberano de cinco países da zona Euro (Portugal, Irlanda, Itália, Grécia e Espanha) seguindo uma abordagem estrutural de primeira passagem em que o movimento Browniano geométrico é substituído por um processo de Lévy regido apenas por uma componente de saltos. Deste modo, introduzimos incrementos assimétricos e leptocúrticos e a possibilidade de incumprimento instantâneo, removendo assim algumas das principais limitações do modelo Black-Scholes.

Calculamos a probabilidade de sobrevivência como preço de uma opção barreira discreta, utilizando um método de valorização de opções baseado na aproximação da densidade de transição como expansão em série de Fourier de cossenos. Assumindo uma taxa de recuperação determinística, calibramos o modelo de Lévy Carr–Geman–Madan–Yor (CGMY) utilizando spreads de Credit Default Swaps semanais e obtemos a estrutura temporal de probabilidades de incumprimento. Tiramos ainda partido da representação do processo Variance Gamma (uma instância do modelo CGMY) como movimento Browniano modificado temporalmente para considerar uma estrutura de dependência entre os riscos de crédito soberanos através de uma modificação temporal comum. Em seguida, ilustramos um possível procedimento de calibração multidimensional e obtemos a distribuição de sobrevivência conjunta via simulação.

Palavras-chave: Risco de crédito; Processos de Lévy; Dívida soberana; Credit Default Swaps; Probabilidade de incumprimento; Expansão em série de Fourier de cossenos; Movimento Browniano modificado temporalmente.

Acknowledgments

I thank my supervisors, João Guerra and Raquel Gaspar, their welcoming, support and commitment.

I thank Joana Martinho her challenge and inspiration.

I am indebted to Manuela Silva for her help and kindness.

I am grateful to Manuel and Guilherme.

Contents

List of Figures

List of Tables

Chapter 1

Introduction

The classical structural approach to corporate credit risk modeling describes the asset value process as a geometric Brownian motion and defines default either as the equity value dropping to zero at maturity (Merton 1974) or as the first passage time of an exogenous default barrier (Black and Cox 1976). It establishes an intuitive relationship between default and the value of a firm's assets, and its dynamics allows the straightforward computation of survival probabilities and the credit spread term structure. However, it is known that the Black-Scholes framework used is unable to capture several well-grounded empirical evidences, such as the skewed and leptokurtic distribution of returns. These shortcomings are rooted in the assumption of Gaussian increments, that imply continuous sample paths. We can overcome them by extending the modeling dynamics to the wider class of Lévy processes. In particular, we can then capture sudden shocks through the introduction of jumps in the asset value process, thereby removing the local predictability of default.

The link between asset value and default is lost when we move from the corporate to the sovereign credit risk realm. Indeed, the estimation of a sovereign asset value process from sound economic fundamentals is still very much an open problem. Additionally, sovereign default can be triggered from strategical political decisions. If a government manages to bridge the gap between the burden of defaulting (such as raising future borrowing costs or facing trade sanctions) and its benefits (immediate debt relief through renegotiation of the original issuance terms), it might find a proper incentive to formally declare default.

In this work, we have not endeavored to address the problem of defining and estimating a suitable sovereign value process. Instead, we co-opt the notion of corporate asset value process and assume that the market price of sovereign default, as measured by the Credit Default Swaps (CDS) spreads term structure, *implicitly* incorporates information on a *latent* sovereign value process. We recognize that the rationale behind this assumption is weaker than the one we could presumably reach had we attempted to devise an explicit sovereign value model. However, as our results will show, this simplified framework will allow us to accurately reproduce the CDS market data both under regular and distress circumstances. We believe this fact upholds our modeling approach.

We propose to model the credit risk of five non core Euro area sovereign bonds (Portugal, Ireland, Italy, Greece and Spain) following the COS method (Fang *et al.* 2010), where a Black-Cox structural approach is taken under Lévy dynamics. We will focus on the Carr–Geman–Madan-Yor (CGMY) process (Carr *et al.* 2002), introduced to support the conjecture that the equity price process should be devoid of a diffusion component. The CGMY model is then a pure jump process, allowing infinite or finite activity regimes. This makes it flexible enough to cope both with high arrival rates of (mostly) small jumps, reflecting pure supply and demand shocks, and sudden, exogenous information shocks. By doing so, we will implicitly be assuming that this asset pricing dynamics is also suitable for

modeling the latent sovereign value process.

The COS method approximates the transition density as a Fourier-cosine series expansion, obtainable from the process characteristic function. It requires only the analytical knowledge of the latter and so provides a tractable and flexible way to compute the survival probability and calibrate Lévy models from CDS market data.

Our main objective is the univariate calibration of the CGMY model and the computation of the implied default probability term structure, spanning the period from January 2010 to the end of February 2014. A secondary goal is the introduction of dependency between the underlying sovereign value processes using the subclass of Lévy processes representable as a time-changed Brownian motion. To this effect, we consider a common time change component. The univariate calibration procedure can be easily adapted to the multidimensional structure, and joint and conditional survival probabilities estimated via simulation.

We believe our work makes three relevant empirical contributions. First, even though we make a strong (and, in a sense, exogenous) assumption on the modeling dynamics, it shows that the CGMY model accurately captures the features of the CDS term structure. The fact that we have used an extensive dataset spanning the main stages of the Euro area sovereign debt crisis further supports the quality of the fit and the model's flexibility. In particular, the calibration has successfully captured extreme behavior under severe distress periods, such as high peaks and inversion effects on the CDS spreads term structure. Secondly, our results provide evidence illuminating the relationship between the data lifecycle and the process structure: namely, a clear switch from an infinite to a finite activity regime under distress. Finally, we provide an extension to a multidimensional setting, incorporating dependency, and illustrate how it can be used to obtain the joint default distribution.

The outline of the text is as follows. Chapter 2 presents the main results of the classical structural approach to corporate credit risk modeling and a brief literature review on possible adaptations to sovereigns. Additionally, it justifies the use of Lévy processes in finance, provides characterization results and introduces the CGMY model and the time-changed Brownian motion representation. Chapter 3 addresses the Fourier-cosine series expansion method underpinning the calibration procedure and the computation of default probabilities. Chapter 4 describes the dataset used and Chapter 5 presents the univariate calibration results. In Chapter 6 we will illustrate the calibration of a multivariate Lévy process by extending the univariate time-changed Brownian motion representation of a specific form of the CGMY process (the Variance Gamma model). Chapter 7 discusses the results and points to future research routes.

Chapter 2

Structural credit risk modeling under Lévy dynamics

2.1 The structural approach

Under the structural approach to corporate credit risk modeling, debt and equity are treated as contingent claims on a firm's asset value process.

2.1.1 The classical Merton approach

In Merton's model (1974), the firm defaults on its debt if the value of the equity drops to zero at the debt's maturity T.[1] The firm's asset value process V_t is modeled as a geometric Brownian motion,

$$dV_t = \mu V_t dt + \sigma V_t dB_t,\ V_0 > 0 \Rightarrow V_t = V_0 \exp\left\{\left(\mu - \frac{1}{2}\sigma^2\right)t + \sigma B_t\right\},$$

where μ is the drift parameter, σ is the volatility and B_t is a standard Brownian.

As the increments of a Brownian motion are normally distributed, the computation of the default probabilities is straightforward:

$$P_{def}(T) = \Phi\left(\frac{\ln\left(\frac{K}{V_0}\right) - \left(\mu - \frac{1}{2}\sigma^2\right)T}{\sigma\sqrt{T}}\right),$$

where K denotes the notional value of the debt.

Merton's model treats equity as a European call option on the value of the firm held by the shareholders, with strike price equal to the outstanding notional value of debt.[2] This leads to Black-Scholes-type formulæ to value the equity and price defaultable bonds.

The limitations of this approach are clear: default can only occur at the debt's maturity T, and the firm value can be arbitrarily close to zero without triggering default.

2.1.2 The first passage approach

Black and Cox's model (1976) overcomes these limitations by introducing an exogenous default barrier D, following the empirical evidence of default events occurring before the equity drops to zero. Default is redefined as the first time the value process V_t hits this barrier. Under the geometric Brownian motion dynamics for V_t, default probabilities are

[1] I.e., if the firm's asset value falls below the outstanding value of the debt.

[2] Likewise, the debt can be seen as a put option.

also easily obtainable, as the distribution of the running minimum of a Brownian motion with drift,

$$\min_{s \leq t} \{\mu s + \sigma B_s\},$$

is known to be Inverse Gaussian. This leads to the following default probability formula (Lando 2004, 259-260):

$$P_{def}(t) = \Phi\left(\frac{\ln\left(\frac{D}{V_0}\right) - \left(\mu - \frac{1}{2}\sigma^2\right)t}{\sigma\sqrt{t}}\right) + \left(\frac{D}{V_0}\right)^{\frac{2\left(\mu - \frac{1}{2}\sigma^2\right)}{\sigma^2}} \Phi\left(\frac{\ln\left(\frac{D}{V_0}\right) + \left(\mu - \frac{1}{2}\sigma^2\right)t}{\sigma\sqrt{t}}\right).$$

We can describe the survival probability as the price of a barrier option without discounting. As a consequence, Black and Cox's model is a natural framework for the application of option pricing techniques.

2.1.3 Drawbacks and desirable properties

The structural approach is conceptually attractive by providing a clear link between default and the firm's asset value process. However, *under the Brownian motion dynamics default is locally predictable*, leading to inconsistencies with intuition and empirical observation. The most striking of these is the unrealistic behavior of the short-term end of the credit spread[3] term structure, which will always approach zero.

A realistic credit risk model should first and foremost treat *default times as locally unpredictable*, which would suggest modeling the firm's asset value using a process with jumps. These could reflect the arrival of new information leading to sudden shocks in the asset value, a behavior that processes with continuous sample paths, such as the Brownian motion, can not capture. Proceeding this way, we would be introducing a mechanism of instantaneous default, thus avoiding artificial techniques to build it into the model such as, for example, making the default threshold barrier stochastic.

In addition, empirical evidence from stock returns suggests that any process describing the firm's asset value should produce a returns distribution with *skewness and positive excess kurtosis (fat-tail behavior)*. This is not consistent with the Gaussian framework of the Black-Scholes model.

Lévy processes, introduced in the next section, provide distributions with these characteristics.

2.1.4 Modeling sovereign debt

We have been describing the structural approach framework under a classical corporate credit risk setting. However, when applying such framework to the problem of modeling sovereign credit risk, we can not interpret V_t as an asset value process in a strict sense, nor can we easily define the default barrier in terms of the outstanding value of debt. This is the main reason why the structural approach is a less trodden path in sovereign credit risk modeling.

A first strand of the literature attempts to define and estimate the sovereign value (or a suitable proxy). Karmann and Maltritz (2003) and Clark and Kassimatis (2004) use the present value of net exports as a measure of a sovereign's market value. This approach might suit developing countries, but it falls short of capturing the sovereign value in advanced economies or countries within a monetary union. Currie and Velandia (2002) produce a stylized government balance sheet: assets are the discounted values of fiscal revenues, foreign reserves and marketable securities; liabilities are the discounted values of government

[3]The difference between yields on defaultable and risk-free bonds.

spending, public debt and contingent liabilities (such as government guarantees, bailouts or deposit insurance schemes). The latter are especially difficult to estimate, as they are linked with the financial performance of the private sector, but the model as a whole is prone to strong forecasting assumptions.

Another strand of the literature discards the direct estimation of the sovereign value and introduces exogenous default indicator processes. Hui and Lo (2002) resort to the foreign exchange rate; Moreira and Rocha (2004) develop accounting ratios involving macro-financial variables. Oshiro and Saruwatari (2005) employ stock indexes as a measure of sovereign "equity" under a classical Black-Scholes structural approach.

A sovereign default event can take several forms: non-payment of principal or interest due, a debt exchange (for claims of lower value), a moratorium or an official repudiation of debt. In contrast to the corporate case, a government might find incentives to default on economic reasons other than the strict ability-to-pay argument that compares the asset value to the outstanding notional of the debt. Strategic political concerns will also play a major role, namely the reputational effect on future borrowing costs and a possible decrease in economic output due to trade sanctions. Along these lines, the default indicator process could reflect the difference between the costs and benefits of default (Eaton and Gersovitz, 1981; Calvo, 1988).

When setting the scope of the current work, we have pragmatically decided not to address the direct estimation of a sovereign value process and focus mainly on the benefits of replacing the geometric Brownian motion dynamics with a suitable Lévy process. As previously mentioned, we will work under the assumption that V_t represents an unobservable sovereign value process, that implicitly determines the CDS spreads term structure and so acts as a default indicator. The default barrier will be redefined in terms of an assumed recovery rate given default and the initial value of the process. Chapter 3 will detail this procedure. In the next section, we address the problem of introducing a suitable Lévy dynamics to model the latent value process V_t.

2.2 Financial modeling with Lévy processes

2.2.1 A brief historical background

Lévy processes have been successfully used in asset pricing models to address some of the main limitations of the Brownian motion dynamics, such as the inability to account for the negative skewed and leptokurtic distribution of log-returns, or the volatility smile[4]. They are a natural generalization of the Brownian motion model, keeping the independence and stationarity of increments, but crucially introducing jumps. These can capture real price discontinuity phenomena and incorporate sudden, unexpected information shocks. In addition, they account for skewness and fat tails.

The non-normality of stock returns was a well established empirical fact as early as 1963, when Maldelbrodt proposed the α-stable class of distributions for stock prices (Mandelbrodt 1963). The Normal distribution is obtained with $\alpha = 2$ and the Cauchy distribution with $\alpha = 1$. When $\alpha < 2$, the density is more peaked around the center than the Gaussian distribution and the variance is infinite, implying fat tails. When $\alpha \leq 1$ the expected value does not exist. The α-stable model is a Lévy model, but empirical evidence has rejected its adequacy to describe stock price returns.

One of the first attempts at introducing discontinuities in the asset price process was the jump-diffusion model of Merton, where a Compound Poisson process with Gaussian jumps

[4]The graphic representation of volatility against option strike prices, constant under the Black-Scholes framework.

is added to a diffusion (Merton 1976). We will briefly illustrate the properties of the jump-diffusion strand of models in Section 2.3, resorting to the Kou model (Kou 2002), where the jumps have a double exponential distribution.

Another strand of Lévy models relies on the Generalized Hyperbolic distribution, introduced by Barndorff-Nielsen (1977) to model the grain size of wind-blown sand. Two particular models of this type are the exponential Hyperbolic motion (Eberlein and Keller 1995) an the exponential Normal Inverse Gaussian (Barndorff-Nielsen 1998). Both have proved capable of accurate fits to empirical stock prices log-returns. Eberlein and Prause (1998) provide a comprehensive account of the family of Generalized Hyperbolic Lévy processes.

The Normal Inverse Gaussian model is a pure jump model with infinite activity[5] and finite variation. It dispenses with a diffusion component and so it has discontinuous sample paths. Local price uncertainty is captured not trough a constant volatility parameter but by the nature of the jumps, arising from pure supply and demand shocks.

More recent efforts have been focusing on the properties of infinite activity and infinite variation pure jump processes. The Variance Gamma model (Madan and Seneta 1990) was successfully used to describe Australian stock market data. The CGMY model (Carr *et al.* 2002) is an extension of the Variance Gamma model accounting for a finer structure of the very small jumps. Interestingly, the pure jump CGMY model has been shown to outperform a modified CGMY model with a diffusion component in describing equity *index* data.[6] We will use the CGMY dynamics to model the latent sovereign value process V_t and discuss its properties in Section 2.4.2. Even though the CGMY model does not present a tractable density function, its characteristic function has an analytic closed form representation. This makes the application of the Fast Fourier Transform (FFT) option pricing method feasible (Carr, Chang and Madan 1998). In fact, we will cast the survival probability problem as an option pricing problem in Chapter 3.

Yet another flavor of the use of Lévy processes in finance is the stochastic volatility model of Barndorff-Nielsen and Shephard (2001). It describes the volatility parameter as a stationary Ornstein-Uhlenbeck process driven by non-Gaussian Lévy increments and addresses the problem of modeling the volatility smile.

An essential result for the multivariate default modeling technique we will develop in Chapter 6 is the representation of a semimartingale as a time-changed Brownian motion (TCBM) (Monroe 1978). In a TCBM, the deterministic time variable is replaced by an independent subordinator.[7] If we take a Lévy subordinator, the TCBM construction will always lead to a Lévy process. This approach shifts the modeling focus to the time-change. The latter can be seen as a stochastic "clock", reflecting the intensity of the economic activity (measured through the accumulated traded volume in the market) and the arrival of new pieces of information (Clark 1973, Ané and Geman, 2000).

Although it is a topic we do not address in this work, we should note that considering independent increments might be too strong an assumption. The fractional Brownian motion model incorporates dependency of increments through a "long-range" dependency property. This means that the covariance between increments decays slowly to zero. However, the application of the fractional Brownian motion to asset pricing problems might be problematic. In particular, the geometric fractional Brownian motion model allows arbitrage opportunities (Rogers 1997).

We now move to define Lévy processes and present some of their basic properties.

[5] As we will detail in the next section, this means that on every compact interval the process has a.s. an infinite number of jumps.

[6] The authors conjecture that possible diffusion components in individual prices are removed when indexes are considered.

[7] An a.s. increasing process independent of the Brownian motion.

2.2.2 Definition and characterization

We start by defining Lévy processes and will then present characterization results that will provide insight into their properties. We will also give some examples widely used in applications to finance and motivate the choice of the CGMY model to describe the latent sovereign asset value (or default indicator) process, V_t.

Let $(\Omega, \mathcal{F}, \mathbb{Q})$ be a filtered probability space and $\mathbf{L} = \{L_t\}_{t\geq 0}$ a càdlàg[8] process.

Definition 2.1 (Lévy process)**.** $\mathbf{L}$ *such that* $L_0 = 0$ *is a Lévy process if*

- $\mathbf{L}$ *has independent increments;*
- $\mathbf{L}$ *has stationary increments;*
- $\mathbf{L}$ *is stochastically continuous:*

$$\forall_{t>0,\,\varepsilon>0}\ \lim_{s\to t} P_{\mathbb{Q}}\left(|L_t - L_s| > \varepsilon\right) = 0.$$

Let $\Delta L_t := L_t - L_{t^-}$ be the jump size of the process at time t. The stochastic continuity condition implies that the times where the jumps occur are random, i.e., we almost surely have $\Delta L_t = 0$. In general, the number of jumps up to time t will not be bounded.

Lévy processes can be identified with the class of infinitely divisible distributions:

Proposition 2.1 (Lévy processes and infinitely divisible distributions)**.** *Let* $\mathbf{L}$ *be a Lévy process.* L_t *has an infinitely divisible distribution*[9] *and, conversely, if* X *is an infinitely divisible distribution, there exists a Lévy process* $\mathbf{L}$ *such that* $L_1 \stackrel{d}{=} X$*.*

The proof can be found in Sato (1999) (Corollary 11.6).

We will describe a Lévy process using its *characteristic function*,

$$\phi_{L_t}(\omega) := \mathbb{E}\left[e^{i\omega L_t}\right] = \int_{\mathbb{R}} e^{i\omega x} f_{L_t}(x)dx, \tag{2.1}$$

which is simply the Fourier transform of the density $f_{L_t}(x)$. The characteristic function can be written as

$$\phi_{L_t}(\omega) = e^{t\psi(\omega)},$$

where ψ is a continuous function referred to as the *characteristic exponent* (Cont and Tankov 2004, Proposition 3.2). Working with the characteristic function is convenient for application purposes because, as we will see, it is easier to obtain analytic formulas for it than for the transition density.

The *Lévy measure* ν is defined as

$$\nu(A) := \mathbb{E}\left[\#\left\{t \in [0,1] :\ \Delta L_t \in A\right\}\right],\ A \in \mathcal{B}(\mathbb{R}),$$

and can be interpreted as the expected number of jumps of size in a given Borel set A, per time unit.

The following result is a central characterization of Lévy processes and provides the intuition underpinning their properties.

Theorem 2.1 (Lévy-Itô decomposition)**.** *Let* $\mathbf{L}$ *be a Lévy process and* ν *its corresponding Lévy measure. Then,*

[8] Right-continuous with left limits.

[9] A random variable X is infinitely divisible if for all $n \in \mathbb{N}$ there exist n i.i.d. random variables $X_j^{(1/n)}$, $j = 1, \ldots, n$, such that $X \stackrel{d}{=} X_1^{(1/n)} + \cdots + X_n^{(1/n)}$.

- *ν is a positive Radon measure on $\mathbb{R}$ such that*

$$\nu(\{0\}) = 0, \quad \int_{|x|\leq 1} x^2 \nu(dx) < \infty, \quad \int_{|x|\geq 1} \nu(dx) < \infty; \tag{2.2}$$

- *L_t can be decomposed in the following sum of independent components:*

$$L_t = L_t^{(1)} + L_t^{(2)} + L_t^{(3)},$$

with

$$\begin{aligned} L_t^{(1)} &:= \gamma t + \sigma B_t \\ L_t^{(2)} &:= \int_{|x|\geq 1,\, s\in[0,t]} x J_X(ds \times dx) \\ L_t^{(3)} &:= \int_{|x|<1,\, s\in[0,t]} x \left[J_X(ds \times dx) - \nu(dx)ds\right], \end{aligned}$$

where

$$J_X([0,t] \times A) = \#\{s \in [0,t] : \Delta L_s \in A\}$$

is a Poisson random measure counting the number of jumps in A up to t.

$L_t^{(1)}$ is a (continuous) Brownian motion with drift γ and volatility σ. Furthermore, every continuous Lévy process is of this form. The second and third components, $L_t^{(2)}$ and $L_t^{(3)}$, provide the jumps, as described by the Lévy measure ν. $L_t^{(2)}$ is a compound Poisson process and $L_t^{(3)}$ is a square integrable martingale that can be seen as an infinite sum of compensated Poisson processes with jump sizes x.

As a corollary of the Lévy-Itô decomposition, we have the following decomposition of the characteristic function $\phi_{L_t}(\omega)$.

Theorem 2.2 (Lévy-Khintchine representation)**.** *The characteristic function of a Lévy process $\phi_{L_t}(\omega)$ has the following representation:*

$$\phi_{L_t}(\omega) = e^{t\psi(\omega)},$$

where

$$\psi(\omega) = i\gamma\omega - \frac{\sigma^2\omega^2}{2} + \int_{\mathbb{R}} \left(e^{i\omega x} - 1 - i\omega x \mathbf{1}_{|x|<1}\right) \nu(dx)$$

is the characteristic exponent of L_1, i.e., $\phi_{L_1}(\omega) = e^{\psi(\omega)}$.

The triplet (γ, σ, ν) is called the Lévy triplet. $\gamma \in \mathbb{R}$ is the drift term, $\sigma > 0$ is the diffusion coefficient and ν is a the Lévy measure, as previously defined.

Details on the previous two results can be found in Cont and Tankov (2004), Section 3.4.

The characteristic exponent can be conveniently written as

$$\psi(\omega) = \psi^{(1)}(\omega) + \psi^{(2)}(\omega) + \psi^{(3)}(\omega),$$

where

$$\begin{aligned} \psi^{(1)}(\omega) &:= i\gamma\omega - \frac{\sigma^2\omega^2}{2} \\ \psi^{(2)}(\omega) &:= \int_{|x|\geq 1} \left(e^{i\omega x} - 1\right) \nu(dx) \\ \psi^{(3)}(\omega) &:= \int_{|x|<1} \left(e^{i\omega x} - 1 - i\omega x\right) \nu(dx) \end{aligned}$$

are the characteristic exponents of, respectively, $L_t^{(1)}$, $L_t^{(2)}$ and $L_t^{(3)}$.

2.2.3 The Lévy measure

The Lévy measure satisfies (2.2) and so it has no mass at the origin, its mass away from the origin is bounded and it can possibly have singularities around the origin. This means that in any compact interval a Lévy process may have infinitely many "small" jumps and at most a finite number of "large" jumps.

The Lévy measure also conveys information on the paths' jumps and variation.

Proposition 2.2 (Lévy measure and the process activity)**.** *Let* $\mathbf{L}$ *be a Lévy process with Lévy triplet* (γ, σ, ν)*.*

- *If* $\nu(\mathbb{R}) < \infty$*,* $\mathbf{L}$ *has finite activity, i.e., almost all paths have a finite number of jumps on any compact interval;*
- *If* $\nu(\mathbb{R}) = \infty$*,* $\mathbf{L}$ *has infinite activity, i.e., almost all paths have a infinite number of jumps on any compact interval.*

Intuitively, we can interpret the fluctuations in a infinite activity process modeling the value of a financial asset as arising from pure supply and demand shocks. In a finite activity process the shocks would be sudden and mostly exogenous, thus incorporating an unexpected arrival of information.

Proposition 2.3 (Lévy measure and the paths' variation)**.** *Let* $\mathbf{L}$ *be a Lévy process with Lévy triplet* (γ, σ, ν)*.*

- *If* $\sigma = 0$[10] *and* $\int_{|x|\leq 1} |x|\nu(dx) < \infty$*, almost all paths of* $\mathbf{L}$ *have finite variation;*
- *If* $\sigma \neq 0$ *or* $\int_{|x|\leq 1} |x|\nu(dx) = \infty$*, almost all paths of* $\mathbf{L}$ *have infinite variation.*

The proofs of the two previous results can be found in Sato (1999) (Theorem 21.3 and 21.9, respectively). For a comprehensive review of the material in this section, with references to standard bibliography on Lévy processes and their application in finance, refer to Papapantoleon (2008).

Having introduced and provided characterization results for Lévy processes, we now move to present some examples relevant for the remainder of the work. Recalling that the key issue in credit risk modeling is how to obtain the survival probability, we observe that to compute it directly we would have to know the distribution of the process running minimum[11], which will not be available in general. However, we will show in Chapter 3 that, by taking advantage of the representation of the characteristic function as a Fourier transform, we can use an efficient algorithm to numerically approximate the transition density (and from it the survival probability). This methodology will only require the knowledge of an analytic expression for the characteristic function.

2.3 Jump-diffusion processes

We have previously mentioned that the Merton jump-diffusion model was one of the first attempts to introduce discontinuities in the price process. Generally speaking, a jump-diffusion Lévy process merges a *diffusion* component with a *finite activity jump process* (i.e., a process such that $\nu(\mathbb{R}) < \infty$, by Proposition 2.2). Thereby, a jump-diffusion has the form

$$L_t = \mu t + \sigma B_t + \sum_{k=1}^{N_t} J_k,$$

[10] I.e., there is no Brownian component.

[11] Or, equivalently, the distribution of its first passage time.

where the term $\mu t + \sigma B_t$, $\mu \in \mathbb{R}$, $\sigma > 0$, is a Brownian motion with drift, and the term $\sum_{k=1}^{N_t} J_k$ is a Compound Poisson process with intensity λ: $N_t \sim \text{Poisson}(\lambda t)$ counts the number of jumps of L_t up to time t, and $J_k \overset{\text{i.i.d}}{\sim} J$ is the distribution of the (independent) jump sizes. Merton's model assumes that J is normally distributed with mean μ_J and variance σ_J^2, and we write this as $J \sim \mathcal{N}\left(\mu_J, \sigma_J^2\right)$.

Kou's model

In Kou's model (2002), the jump size has a double Exponential distribution. The probability density function is then given by

$$f_J(x) = p\theta_1 e^{-\theta_1 x}\mathbf{1}_{\{x>0\}} + (1-p)\theta_2 e^{\theta_2 x}\mathbf{1}_{\{x<0\}},$$

where $0 \leq p \leq 1$ and $\theta_1, \theta_2 > 0$, and we write $J \sim \text{DExp}\left(p, \theta_1, \theta_2\right)$. By the infinite divisibility property of Proposition 2.1, the characteristic function can be written as $\phi_{L_t}(\omega) = \{\phi_{L_1}(\omega)\}^t$, with

$$\phi_{L_1}(\omega) = \exp\underbrace{\left[i\mu\omega - \frac{1}{2}\sigma^2\omega^2\right]}_{\text{Brownian motion}} + \underbrace{\lambda\left(p\frac{\theta_1}{\theta_1 - i\omega} + (1-p)\frac{\theta_2}{\theta_2 + i\omega} - 1\right)}_{\text{Compound Poisson}}. \tag{2.3}$$

The Lévy triplet is simply $\left(\mu, \sigma^2, \lambda \times f_J\right)$.

The density of L_1 is not known in closed form. Kou (2008)[12] provides an implicit way to compute the distribution of the first passage time $\tau := \inf\{t \geq 0 : L_t \geq 0\}$ using its Laplace transform.

2.4 Infinite activity, pure jumps processes

In this section, we discuss processes with no diffusion component (i.e., with volatility parameter $\sigma = 0$) and an infinite activity, pure jump component (thus having $\nu(\mathbb{R}) = \infty$, by Proposition 2.2).

We will start by describing the Variance Gamma process as a Gamma time-changed Brownian motion. We will then present the alternative CGM parametrization, convenient on two different accounts: on the one hand, it illuminates the properties of the underlying Lévy measure; on the other, we can use it to build a natural extension to the CGMY dynamics.

2.4.1 The Variance Gamma process

As a first step, we define the Gamma process $\mathbf{G} = \{G(t)\}_{t\geq 0}$ as a stochastic process with stationary and independent, Gamma distributed[13] increments, such that

- $G(0) = 0$;
- $G(1) \sim \Gamma(a, b) \Rightarrow G(t) - G(s) \sim \Gamma(a(t-s), b),\ 0 < s < t.$

We will refer to (a, b) as the parameters of the Gamma process.

[12] Section 7.3. See also Kou (2002), and Kou, Petrella and Wang (2005).

[13] We use the parametrization of the Gamma distribution whose probability density function is given by $f_{\Gamma(a,b)}(x) = \frac{b^a}{\Gamma(a)}x^{a-1}e^{-bx}$, $x > 0$.

Variance Gamma as a time-changed Brownian motion

Let $\mathbf{B} = \{B(t)\}_{t\geq 0}$ be a standard Brownian motion and $\mathbf{G}$ an *independent* Gamma process with parameters $\left(\frac{1}{\nu}, \frac{1}{\nu}\right)$, $\nu > 0$. The Variance Gamma process (VG) has parameters (σ, ν, θ), $\sigma > 0$, $\theta \in \mathbb{R}$, and is defined as the Gamma time-changed Brownian motion with drift

$$L_t^{VG} := \theta G_t + \sigma B_{G_t}. \tag{2.4}$$

Following Hurd (2009) and Hurd and Zhou (2011), let us denote a Brownian motion with drift by $X_t := \theta t + \sigma B_t$ and a non decreasing, independent Lévy time change by G_t. Let us also consider the induced filtrations

$$\begin{aligned}
\mathcal{W}_t &:= \sigma\left\{B_s : s \leq t\right\}; \\
\mathcal{G}_t &:= \sigma\left\{G_s : s \leq t\right\}; \\
\mathcal{F}_t &:= \sigma\left\{X_s, G_u : u \leq t, s \leq G_t\right\}.
\end{aligned}$$

The characteristic function of $L_t := X_{G_t}$ can be obtained by taking the conditional expectation

$$\begin{aligned}
\phi_{L_t}(\omega) &= \mathbb{E}\left[\mathbb{E}\left[e^{i\omega L_t}|\mathcal{F}_0 \vee \mathcal{G}_t\right]|\mathcal{F}_0\right] \\
&= \mathbb{E}\left[\phi_{X_{G_t}}(\omega)|\mathcal{F}_0\right] \\
&= \phi_{G_t}\left(\theta\omega + \frac{1}{2}i\sigma^2\omega^2\right),
\end{aligned}$$

as $\phi_{X_t}(\omega) = e^{i\theta\omega t - \frac{1}{2}\omega^2\sigma^2 t}$, using the first component of (2.3).

We can then obtain the characteristic function of the Variance Gamma process as

$$\begin{aligned}
\phi_{L_t^{VG}}(\omega) &= \left[\phi_{L_1^{VG}}(\omega)\right]^t \\
&= \left[\phi_{G_1}\left(\theta\omega + \frac{1}{2}i\sigma^2\omega^2\right)\right]^t \\
&= \left(1 - i\theta\nu\omega + \frac{1}{2}\sigma^2\nu\omega^2\right)^{-\frac{t}{\nu}}.
\end{aligned} \tag{2.5}$$

By building the Variance Gamma process as a time-changed Brownian motion, we have replaced the "calendar" time t by the time change G_t, a stochastic "business" time under prevailing market conditions. In a credit risk setting, we can think of the time change as a way to model the arrival of new information. As the market does not forget information, the amount of information cannot decrease, hence the increasing condition on G_t. Intuitively, X_t will represent a default indicator function and the time change G_t a default "intensity".

As a simplifying assumption, we can consider that the amount of new information released will not be affected by the amount of information already available (i.e., that the information process should have independent increments). Moreover, it is also reasonable to require that the information increment depends only on the length of the period involved (stationary increments). This is the motivation behind the use of a non-decreasing information process, with independent and stationary increments. We will be focusing on *Lévy subordinated Brownian motions*, i.e., time-changed Brownian motions (TCBMs) arising by taking G_t to be a non-decreasing, independent Lévy time change, of which the Variance Gamma process is an example. This construction will always lead to a Lévy process.[14]

[14] Although this class of processes is not dense in the general class of Lévy processes (Hurd and Kuznetsov 2009).

One can argue that independence between B_t and G_t is a somewhat restrictive condition; notwithstanding, it provides a flexible enough family of processes for applications while ensuring tractability.

Finally, it is worth mentioning that, as

$$\mathbb{E}[G_1] = 1 \Rightarrow \mathbb{E}[G_t] = t, \tag{2.6}$$

the expected value of the "business" time change equals the "calendar" time.

Under the TCBM construction we will not know in general the distribution of the first passage time.[15] However, if the time change is known explicitly (as is the case with the Variance Gamma process), simulating the process sample paths is a straightforward task, by the TCBM definition. In Chapter 6, we will illustrate a possible extension of the TCBM approach to a multidimensional Variance Gamma framework, and use simulation to estimate joint and conditional default probabilities.

The CGM parametrization

The Variance Gamma process can also be defined as the difference of two *independent* Gamma processes the following way:

$$X_t^{VG} = \underbrace{G_t^{(1)}}_{a=C,\, b=M} - \underbrace{G_t^{(2)}}_{a=C,\, b=G},$$

with $C, G, M > 0$. An explicit mapping between the (σ, ν, θ) and (C, G, M) parameterizations can be found in Cariboni and Schoutens (2009). Using the latter, we can rewrite the characteristic function (2.5) as

$$\begin{aligned}\phi_{L_t^{VG}}(\omega) &:= \varphi_{VG}(\omega) \\ &= \left\{\phi_{L_1^{VG}}(\omega)\right\}^t \\ &= \left(1 - i\frac{\omega}{M}\right)^{-tC}\left(1 + i\frac{\omega}{G}\right)^{-tC}.\end{aligned} \tag{2.7}$$

The Lévy jump measure is given by

$$\nu_{VG}(dx) = \frac{C}{|x|}\left[e^{-Mx}\mathbf{1}_{\{x>0\}}dx + e^{Gx}\mathbf{1}_{\{x<0\}}dx\right], \tag{2.8}$$

and the Lévy triplet is $(\mathbb{E}[L_1], 0, \nu_{VG})$.

Comparing (2.7) with the Lévy-Khintchine decomposition of the characteristic exponent (Theorem 2.2), we see that the VG model is a pure jump process, i.e., with no Brownian component.

From the Lévy measure representation (2.8), we can gather the intuition behind the (C, G, M) parameters. C controls the overall activity intensity, and so the process kurtosis. G and M control the speed at which the jump arrival rates decline with the size of the move (respectively, for negative and positive jumps). Thus they determine the skewness of the process (positive if $G > M$, negative if $G < M$ and zero if $G = M$).

As $\nu_{VG}(\mathbb{R}) = \infty$, on account of the singularity at the origin, we can infer from Proposition 2.2 that the VG process has infinite activity. Lastly, because $\int_{|x|\leq 1} |x|\nu_{VG}(dx) < \infty$, Proposition 2.3 implies that it has finite variation.

The density of the Variance Gamma increments is known explicitly (Cariboni and Schoutens 2009).

[15] To our knowledge, no such result exists either for the Variance Gamma or the CGMY processes.

2.4.2 The CGMY process

The Carr-Geman-Madan-Yor (CGMY) process is a pure jump process accommodating infinite or finite activity regimes. It is a natural extension of the Variance Gamma model, flexible enough to capture both frequent small moves and rare, large jumps in the price process. It was devised by Carr *et al.* (2002) and used to empirically rebut the need of a diffusion component to adequately capture the small movements of asset returns.

It has four parameters, $C > 0$, $G > 0$, $M > 0$ and $Y < 2$. The characteristic function is given by:

$$\begin{aligned}\phi_{L_t^{CGMY}}(\omega) &:= \varphi_{CGMY}(\omega) \\ &= \exp\left\{tC\Gamma(-Y)\left[(M-i\omega)^Y + (G+i\omega)^Y - M^Y - G^Y\right]\right\}. \end{aligned} \tag{2.9}$$

As was the case with the VG process, from the characteristic exponent we easily conclude that it has no Brownian component.

The Lévy measure ν_{CGMY} admits the representation

$$\nu_{CGMY}(dx) = \frac{C}{|x|^{1+Y}}\left[e^{-Mx}\mathbf{1}_{\{x>0\}}dx + e^{Gx}\mathbf{1}_{\{x<0\}}dx\right], \tag{2.10}$$

and the Lévy triplet is given by $(\mathbb{E}[L_1], 0, \nu_{CGMY})$. Comparing (2.8) and (2.10), we see that the introduction of the Y exponent extends the VG Lévy measure by providing an extra measure of control over the fine structure of the process (i.e., the very small jumps, governed by the behavior of the singularity around the origin). Parameters C, G and M play similar roles as before. When $Y = 0$, we recover the VG process.

Observing that

- $\nu_{CGMY}(\mathbb{R}) < \infty$ if and only if $Y < 0$;
- $\int_{|x|\leq 1} |x|\nu_{CGMY}(dx) < \infty$ if and only if $Y < 1$,

Propositions 2.2 and 2.3 show that the Y parameter also controls the process activity and variation. Table 2.1 sums up this conclusion.

Parameter Y	*Properties of the CGMY process*
$Y < 0$	Finite activity, finite variation
$Y = 0$	Variance Gamma process
$0 < Y < 1$	Infinite activity, finite variation
$1 < Y < 2$	Infinite activity, infinite variation

Table 2.1: The parameter Y

We will assume that the dynamics of the latent sovereign value process can be modeled by the CGMY process. In particular, we will set $V_t = V_0 \exp(X_t)$, where X_t is a CGMY process.

In contrast to the VG model, there is no closed form expression for the density of the increments. As a concluding remark, we mention the fact that the CGMY process also admits a time-changed Brownian motion representation, albeit with a time change whose characterization is not as easily attainable as the Gamma process.[16]

[16]The time change can be explicitly characterized through its Laplace exponent (Madan and Yor 2008).

2.5 Jump-diffusions vs. infinity active, pure jump models

When choosing a model, the ability to capture empirical phenomena and the underlying economic motivation must be taken into account. Moreover, we must strike a balance between calibration tractability and the number of parameters used: an increase in the latter will improve accuracy at the expense of the former, as several local optima might be found in a non-linear optimization problem.

The jump-diffusion Kou model offers several advantages from this perspective. On the one hand, it introduces jumps with a double exponential distribution, and so it provides both high peaks (capturing the underreaction to new information the market receives) and heavy tails (reflecting overreaction). On the other, it provides analytic tractability through the Laplace transform of the first passage time distribution. However, by using a jump-diffusion process we loose the flexibility a infinite activity process might afford.

We have chosen the CGMY model over a jump-diffusion of the Kou type taking into account the following arguments:

- it captures the stylized empirical behavior of asset returns;
- the pure jump nature of the process is adequate both for stable (an infinite number of "small" jumps in a given time interval) and sudden, low frequency changes in market behavior (at most a finite number of "big" jumps in a given time interval);
- through parameter Y both finite and infinite activity processes are attainable, thus possibly capturing breaches in prevailing market conditions through the crossing of the activity regime;
- even though analytic tractability is lost, in Chapter 3 we will describe an efficient numerical method for the computation of survival probabilities, requiring only the explicit knowledge of the parametric characteristic function (2.9);
- it allies flexibility and numerical tractability to a lower number of parameters.[17]

Furthermore, we advocate that the pure jump, infinite activity modeling approach is conceptually sounder than the jump-diffusion one. Indeed, the latter adds an orthogonal jump component, essentially capturing "large", rare jumps that introduce discontinuities, to a diffusion, seizing frequent and small increments. Empirical evidence shows that this can breach the density's monotonicity, on either side of the increments' distribution. A pure jump, infinite activity model dispenses with this unconnected building block, effectively merging the small scale behavior (an infinite number of "small" jumps on any compact interval if the Lévy measure ν is not bounded around the origin) with the large scale jumps (finitely many, as the Lévy measure is always bounded away from zero). This way, it favors smooth, monotone densities on the right and left of the distribution, displaying skewness and heavy tails.

[17] The CGMY model has four parameters, C, G, M and Y. Kou's model has six parameters, p, θ_1, θ_2, λ, μ and σ.

Chapter 3

Univariate default modeling: the COS method

In this chapter we address the problem of computing the survival probability under a Lévy first passage structural approach. We will also show how to price Credit Default Swaps (CDSs) and calibrate the underlying model to CDS spreads market data.

Our modeling framework quite naturally casts the survival probability as the price of a barrier option. As such, we can resort to numerical option pricing techniques to compute it. We will apply the Fourier-cosine series option pricing method (Fang and Oosterlee 2008, 2009), henceforth simply referred to as the COS method. This method approximates the transition density $f_{X_t|X_s}(y|x)$, truncated to a suitably chosen closed interval $[a, b]$, as a Fourier-cosine series expansion.[1] The crucial observation behind it is the fact that the characteristic function is simply the Fourier transform of the probability density. To obtain the Fourier cosine-series coefficients, we will only need to know an analytic expression for the characteristic function. By using a grid of monitoring points, we can recursively compute the survival probability. This approach is convenient as the Lévy density function $f_{X_t}(x)$ might not be known in closed form, whereas generally we can obtain the characteristic function $\phi_{X_t}(\omega)$.

The material we cover closely follows Fang *et al.* (2010), where the COS method is used to price CDSs and, through it, calibrate Lévy models. Although we will be applying the COS method to the calibration of the CGMY model, using the parametric expression (2.10), we should emphasize that it could be used at no further cost to any Lévy process whose characteristic function is analytically obtainable.

3.1 Overview

Under a risk-neutral setting, we consider a latent sovereign value process $\{V_t,\ t \geq 0\}$, where

$$V_t = V_0 e^{X_t}$$

and $\{X_t,\ t \geq 0\}$ is a Lévy process with $X_0 = 0$. We say that V_t is an *exponential Lévy process*.

For a given *deterministic recovery rate* $R \in (0, 1)$, the *time of default* is defined as the first-passage time for a barrier set at $R\,V_0$:

$$\tau_{def} := \inf \{t \geq 0 :\ V_t \leq R\,V_0\}\,.$$

[1] The Fourier-cosine series outperforms the usual Fourier series expansion when approximating functions with compact support (Fang and Oosterlee 2008).

This modeling choice takes the following intuition into account: the larger the recovery rate R, the lower the cost of defaulting incurred by the sovereign, and so the higher its incentive to formally declare default.[2]

The survival probability up to time t is then

$$P_{surv}(t) = \mathbb{P}_{\mathbb{Q}}\left(\min_{0\le s\le t} X_s > \ln R\right) = \mathbb{E}_{\mathbb{Q}}\left[\mathbf{1}_{\left\{\min_{0\le s\le t} X_s > \ln R\right\}}\right], \tag{3.1}$$

where $\mathbb{Q}$ denotes the risk-neutral measure. Equation (3.1) can be interpreted as the price of a binary down-and-out barrier (BDOB) option without discounting, with maturity T and barrier level $h \equiv \ln R$. This option pays one unit currency if the trajectory of the process $\{X_t\}$ remains above h up to time T and zero otherwise. As discussed in Chapter 2, we should note that the distribution of the running-minimum $\min_{0\le s\le t} X_s$ in (3.1) will not generally be known.

3.2 Transition density

The following proposition is the main result behind the COS method.

Proposition 3.1 (COS formula for the transition density)**.** *Let $\{X_t,\ t \ge 0\}$ be a Lévy process with characteristic function $\varphi_{levy}(\omega, t) := \phi_{X_t}(\omega)$. For $0 \le s \le t$ and $x, y \in [a, b] \subset \operatorname{supp} f_{X_t|X_s}$, the Fourier-cosine series of the transition density $f_{X_t|X_s}(y|x)$ can be approximated by*

$$f_{X_t|X_s}(y|x) = \frac{2}{b-a}\sum_{k=0}^{N-1}{}'\operatorname{Re}\left\{\varphi_{levy}\left(\frac{k\pi}{b-a}, t-s\right)e^{ik\pi\frac{x-a}{b-a}}\right\}\cdot\cos\left(k\pi\frac{y-a}{b-a}\right) + \varepsilon_f, \tag{3.2}$$

where $\sum'$ means that the first term is halved. The error term ε_f comes both from truncating the support of $f_{X_t|X_s}$ to the interval $[a, b]$ and taking only the first N terms of the series expansion.

Appendix A.1 presents the proof of this result.

3.3 Survival probability

In this section we will show how the transition density approximation formula (3.2) can be used to compute the survival probability $P_{surv}(t)$ as the price of a discretely monitored binary down-an-out barrier option.

We start by defining a set of M pre-specified observation dates,

$$\mathcal{T} = \{t_0, t_1, \ldots, t_M\},\ t_0 < t_1 < \cdots < t_M,\ t_m = m\cdot\Delta t,\ m = 0, 1, \ldots, M,$$

where the value of the Lévy process $\{X_t,\ t \ge 0\}$ will be monitored and compared with the barrier level set at $h \equiv \ln R$. We will denote the final observation date by $\tau = t_M$.

The survival probability for the whole period

$$P_{surv}(\tau) = \mathbb{E}_{\mathbb{Q}}\left[\prod_{m=0}^{M}\mathbf{1}_{\{X_{t_m} > h\}}\right] \tag{3.3}$$

[2]The default barrier is defined in terms of a relative decrease of the latent sovereign value process so as to avoid the need to explicitly estimate V_0. Following the remarks made in Section 2.1.4, we acknowledge the fact that this choice is made on pragmatic grounds rather than economic or financial fundamentals.

can be obtained recursively. Define

$$\begin{aligned} p(x,t_M) &:= \mathbf{1}_{\{x>h\}} \\ p(x,t_m) &:= \mathbb{E}_{\mathbb{Q}}\left[\mathbf{1}_{\{X_{t_{m+1}}>h\}}\middle| X_{t_m}=x\right] \\ &= \int_h^{+\infty} f_{X_{t_{m+1}}|X_{t_m}}(y|x)p\left(y,t_{m+1}\right)dy, \end{aligned} \tag{3.4}$$

for $m = M-1,\ldots,0$. Then, by taking conditional expectations on the values of X_{t_m} in (3.3), we get

$$P_{surv}(\tau) = p(0,t_0), \tag{3.5}$$

because, from our definition of the sovereign value process V_t, $X_0 = 0$.

We will now use the COS expansion of the transition density from the previous section to approximate the recursive integral in (3.4).

Proposition 3.2 (COS formula for the survival probability)**.** *Plugging (*3.2*) into (*3.4*), we get the following recursive relationship:*

$$p(x,t_m) = {\sum_{k=0}^{N-1}}' \phi_k(x)P_k(t_{m+1}),$$

where

$$\begin{aligned} \phi_k(x) &:= \mathrm{Re}\left\{\varphi_{levy}\left(\frac{k\pi}{b-a},\Delta t\right)e^{ik\pi\frac{x-a}{b-a}}\right\} \\ P_k\left(t_{m+1}\right) &:= \frac{2}{b-a}\int_h^b \cos\left(k\pi\frac{y-a}{b-a}\right)p\left(y,t_{m+1}\right)dy. \end{aligned}$$

The survival probability can then be approximated by

$$P_{surv}(\tau) = {\sum_{k=0}^{N-1}}' \phi_k(0)P_k(t_1). \tag{3.6}$$

The proof can be found in Appendix A.2.

We should note that $\{P_k\left(t_1\right)\}_{k=0}^{N-1}$ are simply the Fourier-cosine coefficients of $p(y,t_1)$. In the next section we will show how these can be computed recursively.

3.3.1 Backwards recursion

The Fourier coefficients $\{P_k\left(t_m\right)\}_{k=0}^{N-1}$ can be obtained from $\{P_k\left(t_{m+1}\right)\}_{k=0}^{N-1}$ the following way:

$$\begin{aligned} P_k(t_m) &= \frac{2}{b-a}\int_h^b \cos\left(k\pi\frac{y-a}{b-a}\right)p\left(y,t_m\right)dy \\ &= \frac{2}{b-a}\int_h^b \cos\left(k\pi\frac{y-a}{b-a}\right){\sum_{l=0}^{N-1}}'\phi_l(x)P_l(t_{m+1})dy \\ &= {\sum_{l=0}^{N-1}}'\mathrm{Re}\left\{\varphi_{levy}\left(\frac{l\pi}{b-a},\Delta t\right)\omega_{kl}\right\}P_l(t_{m+1}), \end{aligned}$$

where we have defined

$$w_{kl} := \frac{2}{b-a}\int_h^b e^{il\pi\frac{y-a}{b-a}}\cos\left(k\pi\frac{y-a}{b-a}\right)dy.$$

In matrix notation, the previous recursive relationship becomes

$$\mathbf{P}(t_m) = \mathrm{Re}\{\Omega\Lambda\}\,\mathbf{P}(t_{m+1}), \tag{3.7}$$

where

$$\Omega = (\omega_{kl})_{k,l=0}^{N-1} \text{ and } \Lambda = \mathrm{diag}\left\{\varphi_{levy}\left(\frac{l\pi}{b-a}, \Delta t\right)\right\}_{l=0}^{N-1}$$

is a diagonal matrix.

So, the computation of the survival probability up to $\tau = t_M$ using the COS formula (3.6) boils down to obtaining the vector of Fourier-cosine coefficients $\mathbf{P}(t_1)$ from the backwards recursion

$$\mathbf{P}(t_1) = \mathrm{Re}\{\Omega\Lambda\}^{M-1}\mathbf{P}(t_M). \tag{3.8}$$

The recursion base vector of Fourier-cosine coefficients for $p(x, t_M) = \mathbf{1}_{\{x>h\}}$, $\mathbf{P}(t_M)$, can be calculated explicitly as

$$\begin{aligned} P_k(t_M) &= \frac{2}{b-a}\int_h^b \cos\left(k\pi\frac{y-a}{b-a}\right)\underbrace{p(y,t_M)}_{\mathbf{1}_{\{y>h\}}}dy \\ &= \begin{cases} \frac{2}{k\pi}\left[\sin(k\pi) - \sin\left(k\pi\frac{h-a}{b-a}\right)\right] & k \neq 0 \\ \frac{2}{b-a}(b-h) & k = 0, \end{cases} \end{aligned} \tag{3.9}$$

but getting the coefficients $\mathbf{P}(t_1)$ using (3.8) is computationally expensive.

In the next section we will describe an alternative, more efficient way to compute (3.8) using the Fast Fourier Transform (FFT) algorithm.

3.3.2 Computation using the FFT

The crucial observation is the fact that the matrix Ω can be expressed as the sum of two matrices with special properties. To see this, first define

$$w_j := \begin{cases} i\pi\frac{b-h}{b-a} & j = 0 \\ \frac{\exp(ij\pi) - \exp\left(ij\frac{h-a}{b-a}\pi\right)}{j} & j \neq 0. \end{cases}$$

Proposition 3.3 (Representation of Ω as the sum of Hankel and Toeplitz matrices)**.** *The matrix Ω can be written as*

$$\Omega = -\frac{i}{\pi}(H + T),$$

where

$$H = \begin{bmatrix} w_0 & w_1 & \cdots & w_{N-2} & w_{N-1} \\ w_1 & w_2 & \cdots & \cdots & w_N \\ \vdots & \iddots & \iddots & \iddots & \vdots \\ w_{N-2} & w_{N-1} & \cdots & \cdots & w_{2N-3} \\ w_{N-1} & \cdots & \cdots & w_{2N-3} & w_{2N-2} \end{bmatrix} \text{ and } T = \begin{bmatrix} w_0 & w_1 & \cdots & w_{N-2} & w_{N-1} \\ w_{-1} & w_0 & \cdots & \cdots & w_{N-2} \\ \vdots & \ddots & \ddots & \ddots & \vdots \\ w_{2-N} & w_{3-N} & \cdots & \cdots & w_1 \\ w_{1-N} & \cdots & \cdots & w_{-1} & w_0 \end{bmatrix}$$

are, respectively, a Hankel *matrix*[3] *and a* Toeplitz *matrix,*[4] *both $N \times N$.*

[3] A Hankel matrix $H = (h_{ij})_{i,j=1}^N$ is a square matrix with constant positive slope diagonals, i.e., such that $h_{ij} = h_{i-1,j+1}$.

[4] A Toeplitz matrix $T = (t_{ij})_{i,j=1}^N$ is a square matrix with negative positive slope diagonals, i.e., such that $t_{ij} = t_{i+1,j+1}$.

Details on the proof can be found in Fang and Oosterlee (2009), pp. 8-9.

The basic recursion for the recovery of the Fourier-cosine coefficients (3.7) can then be rewritten[5] as

$$\mathbf{P}(t_m) = \frac{1}{\pi}\mathrm{Im}\left\{(H+T)\,\mathbf{u}(t_{m+1})\right\}, \tag{3.10}$$

with $\mathbf{u}(t_{m+1}) := (u_j(t_{m+1}))_{j=0}^{N-1}$ such that

$$u_0(t_{m+1}) := \frac{1}{2}\varphi_{levy}(0,\Delta t)\,P_0(t_{m+1}) \tag{3.11}$$

$$u_j(t_{m+1}) := \varphi_{levy}\left(\frac{j\pi}{b-a},\Delta t\right)P_j(t_{m+1}),\ j=1,\ldots,N-1. \tag{3.12}$$

Due to the structure of Hankel and Toeplitz matrices, their product by a vector can be expressed as a *circular convolution*. This will allow us to recover $\mathbf{P}(t_m)$ using the FFT algorithm, thus significantly reducing the complexity of the computation.

Definition 3.1 (Circular convolution)**.** *Take two vectors of the same dimension,* $\mathbf{x}$ *and* $\mathbf{y}$*, and denote by* $\mathcal{D}$ *the discrete Fourier transform (DFT) operator. The circular convolution of* $\mathbf{x}$ *and* $\mathbf{y}$ *is*

$$\mathbf{x}\circledast\mathbf{y} := \mathcal{D}^{-1}\left\{\mathcal{D}(\mathbf{x})\cdot\mathcal{D}(\mathbf{y})\right\}.$$

Proposition 3.4. *Let* H *and* T *be, respectively, Hankel and Toeplitz* $N\times N$ *matrices.*

1. *The matrix-vector product* $H\cdot\mathbf{u}$ *can be obtained as*

$$H\cdot\mathbf{u} = \left[\mathbf{w}_H\circledast\mathbf{u}_H\right]^{\overleftarrow{N}}$$

with the following vectors of dimension $2N$

$$\mathbf{w}_H := [w_{2N-1}, w_{2N-2},\ldots,w_1,w_0]^T \tag{3.13}$$

$$\mathbf{u}_H := [0,\ldots,0,u_0,u_1,\ldots,u_{N-1}]^T, \tag{3.14}$$

where $[\mathbf{x}]^{\overleftarrow{N}}$ *denotes taking the vector of the first* N *elements of* $\mathbf{x}$*, in reversed order.*

2. *The matrix-vector product* $T\cdot\mathbf{u}$ *can be obtained as*

$$T\cdot\mathbf{u} = \left[\mathbf{w}_T\circledast\mathbf{u}_T\right]^{\overrightarrow{N}}$$

with the following vectors of dimension $2N$

$$\mathbf{w}_T := [w_0,w_{-1},\ldots,w_{1-N},0,w_{N-1},w_{N-2},\ldots,w_1]^T \tag{3.15}$$

$$\mathbf{u}_T := [u_0,u_1,\ldots,u_{N-1},0,\ldots,0,]^T, \tag{3.16}$$

where $[\mathbf{x}]^{\overrightarrow{N}}$ *denotes taking the vector of the first* N *elements of* $\mathbf{x}$*.*

The proof can be found in Fang and Oosterlee (2009) – first part – and Almendral and Oosterlee (2007) – second part.

Remark (*Decreasing the complexity of the computation of the Fourier-cosine coefficients*). The matrix-vector products in equation (3.7) involve $\mathcal{O}\left(N^2\right)$ operations. Using (3.10) and the previous proposition, we can reduce it to $\mathcal{O}(N\log_2 N)$, as the complexity of the FFT algorithm is of this order.

[5] $z\in\mathbb{C}$ can be written as $z = |z|e^{i\theta} = |z|\left[\cos(\theta)+i\sin(\theta)\right]$, for a unique argument $\theta\in[0,2\pi[$, and so $\mathrm{Re}(-iz) = |z|\left[\sin(\theta)-i\cos(\theta)\right] = |z|\sin(\theta) = \mathrm{Im}(z)$.

3.3.3 The COS algorithm

This sections outlines the main steps of the COS algorithm to compute the survival probability $P_{surv}(\tau)$, $\tau = t_M$.

Recursion base

Step 1 Compute $\mathbf{P}(t_M)$, the vector of Fourier-cosine coefficients of $p(x, t_M)$, from (3.9);

Step 2 Build the vectors $\mathbf{w}_H$ and $\mathbf{w}_T$ from (3.13) and (3.15);

Step 3 Compute the FFTs $\mathbf{d}_H = \mathcal{D}(\mathbf{w}_H)$ and $\mathbf{d}_T = \mathcal{D}(\mathbf{w}_T)$;

Recursion loop

For $m = M, \ldots, 2$, perform the following steps:

Step 4 Compute the vector $\mathbf{u}(t_m)$ from (3.11) and (3.12);

Step 5 Compute $\mathbf{u}_H(t_m)$ from (3.14);

Step 6 Compute the matrix-vector products

$$H \cdot \mathbf{u}(t_m) = \left[\mathcal{D}^{-1}\left\{\mathbf{d}_H \cdot \mathcal{D}\left[\mathbf{u}_H(t_m)\right]\right\}\right]^{\overleftarrow{N}}, \quad T \cdot \mathbf{u}(t_m) = \left[\mathcal{D}^{-1}\left\{\mathbf{d}_T \cdot \mathcal{D}\left[\mathbf{u}_H(t_m)\right]\right\}\right]^{\overrightarrow{N}};$$

Step 7 Obtain $\mathbf{P}(t_{m-1})$ from (3.10);

At the end of the loop, we will have recovered $\mathbf{P}(t_1)$, the vector of Fourier-cosine coefficients of $p(x, t_1)$.

Survival probability

Step 8 Compute the survival probability $P_{surv}(\tau)$ from (3.6).

Improving the computational efficiency

Coefficients w_j The coefficients w_j must be computed for

$$j = \underbrace{-(N-1), \ldots, -1}_{N-1 \text{ terms}},\ j = 0,\ j = \underbrace{1, \ldots, N-1}_{N-1 \text{ terms}},\ j = \underbrace{N, \ldots, 2(N-1)}_{N-1 \text{ terms}}.$$

To do so in an efficient way, we note that, from the definition, $w_{-j} = -\overline{w_j}$, and so we can get w_j for $j = -(N-1), \ldots, 1$ from w_j, $j = 1, \ldots, N-1$. Additionally,

$$w_{j+N} = \frac{\exp(iN\pi)\exp(ij\pi) - \exp\left(iN\frac{h-a}{b-a}\pi\right)\exp\left(ij\frac{h-a}{b-a}\pi\right)}{N+j},$$

so the factors $\exp(ij\pi)$ and $\exp\left(ij\frac{h-a}{b-a}\pi\right)$ need to be computed only once.

FFT As $\mathbf{u}_H$ is simply $\mathbf{u}_T$ shifted N positions to the right, the FFT $\mathbf{d}_H$ can be computed from $\mathbf{d}_T$, using the shift property of the discrete Fourier transform:

$$\mathcal{D}(\mathbf{u}_H) = \mathbf{sgn} \cdot \mathcal{D}(\mathbf{u}_T), \quad \mathbf{sgn} = \left[(-1)^j\right]_{j=0,\ldots,2N-1}.$$

3.4 Pricing Credit Default Swaps

In a Credit Default Swap (CDS) contract, the protection buyer transfers the credit risk of a reference entity's underlying asset to the protection seller by paying a premium until a default event occurs or the maturity of the contract is reached. The protection seller makes no payments in the latter case, while it covers the losses in case of default. The *CDS spread* is the yearly rate paid by the protection buyer. It thereby provides the market a *quantitative measure of the implicit credit riskiness of the reference entity.*

Let us denote by T the maturity of a CDS contract with yearly spread c. We will assume a constant risk-free interest rate r in $[0,T]$, and that a deterministic recovery rate $R \in (0,1)$ is known in advance.[6]

Proposition 3.5. *The fair CDS spread can be approximated as*

$$c^* = (1-R)\left[\frac{1-e^{-rT}P_{surv}(T)}{\sum_{j=0}^{J} w_j e^{-r\tilde{t}_j} P_{surv}\left(\tilde{t}_j\right)\cdot \Delta t} - r\right], \tag{3.17}$$

where $\tilde{t}_j = j\cdot\Delta t$, $j=0,\ldots,J$, $\Delta t = \frac{T}{J}$, *is a suitable discretization of the interval* $[0,T]$, *and* $w_j = \frac{1}{2}$ *for* $j=0,J$, $w_j = 1$ *otherwise.*

We prove this result in Appendix A.3.

Equation (3.17) shows that we can numerically approximate the fair CDS spread by computing the survival probability $P_{surv}(\tilde{t}_j)$ for every $\tilde{t}_j$. We will use the COS survival probability formula (3.6) for a given Lévy process, as specified by its parametric characteristic function. In the next section, we will define the procedure to calibrate the parameters of the latter to market CDS spread data.

Remark (*Simultaneous computation of survival probabilities*). The choice of the points $\tilde{t}_j$ used to approximate the integral on the CDS pricing formula can be made in such a way that the computation of *all* the survival probabilities $P_{surv}\left(\tilde{t}_j\right)$ is achievable simultaneously. For this, we simply need to ensure that the J points $\left\{\tilde{t}_j\right\}_{j=1}^{J}$ lie in the set of M observation dates $\{t_j\}_{j=0}^{M}$ used in the discretization of the barrier option. If $\tilde{t}_i < \tilde{t}_j$ are two such points, we have $t_i = \frac{k}{M}t_j$ for some $k \in \mathbb{N}$, and so the Fourier-cosine coefficients of the survival probability $P_{surv}(t_i)$ were already obtained during the computation of $P_{surv}(t_j)$:

$$\mathbf{P}_{\tilde{t}_i}(t_1) = \mathbf{P}_{\tilde{t}_j}(t_{M-k+1}).$$

3.5 Calibration

Let $\varphi_{levy}(\omega,t;\theta_1,\ldots,\theta_n)$ be the characteristic function of the underlying Lévy process $\{X_t\}_{t\geq 0}$, with parameters $\theta_1,\ldots,\theta_n$.

On a given day, we observe the market CDS spreads $c_{market}(T_i)$ for a set of m maturities $T_1 < \cdots < T_m$. We will calibrate the Lévy model to the market data by minimizing the root mean square error function

$$\mathrm{RMSE}(\theta_1,\ldots,\theta_n) = \sqrt{\sum_{i=1}^{m}\frac{\left(c_{market}(T_i) - c_{levy}(T_i)\right)^2}{m}}, \tag{3.18}$$

where $c_{levy}(T_i)$ is computed using the COS formula (3.17). The optimal choice of parameters,

$$\mathrm{argmin}_{\theta_1,\ldots,\theta_n}\mathrm{RMSE}(\theta_1,\ldots,\theta_n),$$

will be obtained using the `fmincon` non-linear numerical optimization method in MATLAB®.

[6] It is out of the scope of the present work to address the stochastic modeling of sovereign recovery rates.

3.6 Parameters

Discretization parameters

Following the error analysis discussed in Fang *et al.* (2010), we use the authors' proposed choice of discretization parameters:

Parameter	*Description*	*Value*
N	Terms in Fourier-cosine series expansion	$N = 2^{10}$
M	Monitoring dates for discrete BDOB option	$M = 48T$
J	Discretization points for CDS pricing	$J = \frac{M}{4}$

Table 3.1: Discretization parameters

N The number of terms in the Fourier-cosines series expansion N is chosen as a power of two to allow the use of the FFT algorithm; we use $N = 2^{10} = 1024$ terms;

M We will be using weekly-monitored survival probabilities; $M = 48T$ (or, equivalently, $\Delta t = \frac{1}{48}$) means we are considering 48 "trading weeks" in a year;

J The authors find the CDS pricing formula not to be very sensitive to this parameter; the choice $J = \frac{M}{4}$ (as opposed to $J = M$) is used to improve computational efficiency.

Truncation range

The truncation range of the support of the transition density $f_{X_t|X_s}$ should made be large enough for the approximation error term in (3.2) to stem mainly from taking only N terms in the Fourier-cosine series (Fang *et al.* 2010). The authors find the following definition to be wide enough:

$$[a, b] := \left[c_1 \pm L\sqrt{c_2 + \sqrt{c_2}} \right],$$

where c_j is the j-th cumulant of X_t (cf. Fang and Oosterlee 2009, appendix B) and parameter $L \in [7.5, 10]$. We have used $L = 10$.

Recovery rate

We have decided from the beginning that taking a stochastic modeling approach to the recovery rate parameter R would be out of our work's scope. Arguably, we could assume that R follows a given parametric distribution, with minimal implementation effort.[7] However, such a modeling choice would be made mainly on practical arguments rather than sound economic reasoning. Moreover, we would have to calibrate the distribution parameters making some crude assumptions: data on sovereign loss given default is not only scarce, precluding any statistically significant analysis, but also heterogeneous, as final recovery rates will be determined by the specific economic and political circumstances leading to default.

Because we are strictly focused on Euro area sovereigns, we will use available data on the 2012 Greek and 2013 Cypriot defaults as a proxy for a non-deterministic Euro area recovery rate. These default events have taken the form of distressed debt exchanges[8], as opposed to missing payments of coupons or principal. In its report on *Sovereign Default and Recovery Rates, 1983–2013* (Moody's Investors Service 2014), Moody's measures the recovery rate as

[7] Two possible models are the Beta distribution (with support $[0, 1]$) or an appropriate map of a distribution with support $\mathbb{R}$ to $[0, 1]$ (Schönbucher 2003, Section 6.1.6).

[8] Implying lower values of coupons or par amounts, lower seniority or longer maturities.

the ratio of the present value[9] of the new, restructured securities to the original ones. Table 3.2 presents the estimated recovery rates and the value of the restructured securities. The latter is also expressed as a percentage of both the country's total debt and its GDP.

Year	*Country*	*R (%)*	*% Total Debt*	*% GDP*	*Value ($bn)*
2012	Greece	29	59	98	273
2012	Greece	40	9	15	42
2013	Cyprus	53	6	6	1.3

Table 3.2: 2012–2013 Euro area default events. Source: Moody's *Sovereign Default and Recovery Rates, 1983–2013.*

Taking into account the sheer dimension of the first 2012 Greek restructuring[10], we will choose a deterministic recovery rate of 30%. The data on the Cyprus default suggests that our choice is possibly conservative.

[9] Using the original securities' yield to maturity at the time of the exchange.

[10] The largest in history, measured as the nominal amount of debt exchanged, the percentage of total debt and the ratio to GDP.

Chapter 4

The dataset

As we have seen in the previous chapter, to calibrate a Lévy model from market CDS spreads we will need to minimize the root mean square error (3.18) of the theoretical spreads vis-a-vis the observed ones. This means that, besides fetching market CDS data, we will need information on the risk-free yield curve to use the pricing formula (3.17).

We have collected from Bloomberg the series of daily bid and ask USD-quoted CDS spreads with maturities $T \in \{1, 3, 5, 7, 10\}$ years (Y), spanning the period from 01-01-2010 to 28-02-2014, for the Euro-area Portuguese (PT), Irish (IE), Italian (IT), Greek (GR) and Spanish (SP) sovereigns. This time frame covers the onset of the Euro-area sovereign debt crisis, its peak, and the early stages of the ongoing recovery. To remove possible weekday effects, our calibration will be based only on weekly Wednesday mid-quotes.

We used USD-quoted CDS spreads because the corresponding Euro-quoted ones did not cover extensively neither the period in question nor a representative set of tenors.[1] We recognize that, ideally, Euro-quoted CDS contracts should be used, as the underlying sovereign debt is Euro-denominated. However, the USD dataset was judged preferable, as it would lead to a statistically more significant calibration. We are thus taking the perspective of an American investor in Euro-area sovereign debt. Furthermore, as the recovery rate R is purely exogenous, *we will assume that it covers not only the notional loss given default but also any foreign exchange losses.* This simplifying assumption will give leeway to the use of USD-quoted spreads as a pure credit risk measure, free of any implicit currency risk component.

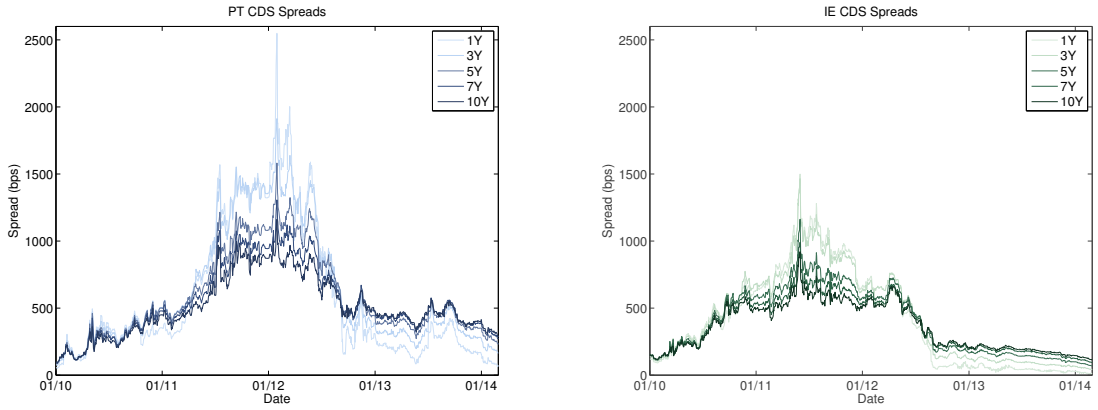

Figure 4.1: Daily mid-quotes for Portuguese (PT) and Irish (IE) CDS spreads

Figure 4.1 shows that the Portuguese and Irish CDS spreads had a somewhat similar

[1] Only the 5 and 10 years tenors were generally available. This is an indication of the Euro denominated market's lower liquidity and depth, when compared the USD one.

behavior, the latter lagging the former, albeit with a lower short-term, 1 year maturity peak. A clear term structure "inversion" effect is noticeable on both series around their peaks, when the short-term spreads become significantly larger than the long-term ones. This is consistent with the dramatic increase in short-term default expectations while the Euro area sovereign debt crisis unfolded. Another noticeable feature is the almost parallel running of most of the tenors *before* the "inversion" effect (onset of the crisis), and a clear separation of the term structure afterwards (beginning of the recovery). These two empirical findings suggest that we will need a flexible enough dynamics for the implicit sovereign value process, an observation further supporting the choice of the CGMY model. Indeed, we should mention that we have chosen this dataset as a means to investigate the relationship between the time series features we have just described and the structural properties of the CGMY process.

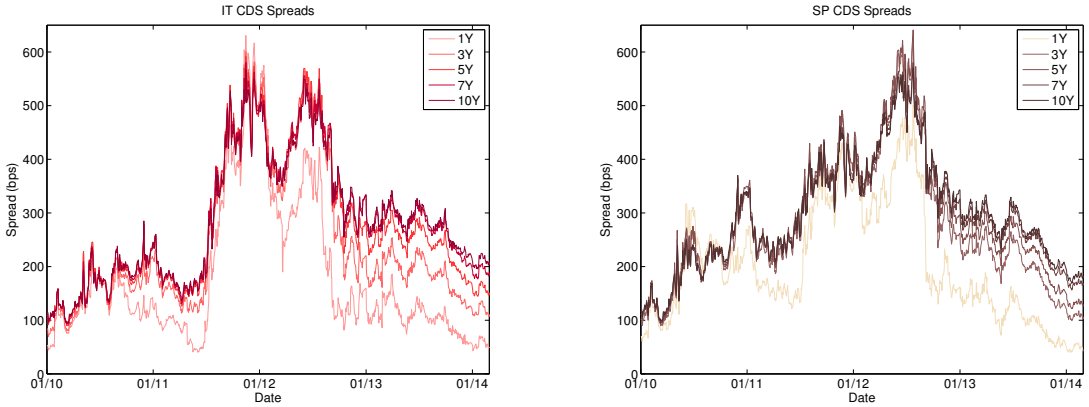

Figure 4.2: Daily mid-quotes for Italian (IT) and Spanish (SP) CDS spreads

The behavior of the Italian and Spanish spreads is also quite similar, although the "inversion" effect does not take place. The "separation" effect at the end of the series is again noticeable. The Greek series mimics the Portuguese CDS spreads lifecycle, with severe distress features: the short term 1 year CDS spread peaks at around 60%.[2]

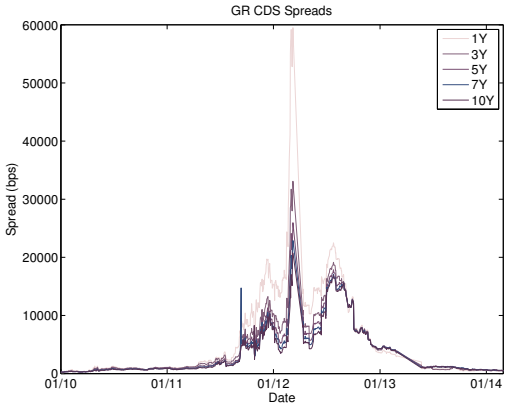

Figure 4.3: Daily mid-quotes for Greek (GR) CDS spreads.

We used the US Treasury yield data[3], providing the daily treasury zero curve for terms $\left\{\frac{1}{12}, \frac{1}{4}, \frac{1}{2}, 1, 2, 3, 5, 7, 10, 20, 30\right\}$ years. In the CDS pricing formula (3.17), r will be the rate corresponding to the calibration date and the CDS tenor T.

[2]The series is broken between 2012-03-12 and 2012-04-10 and again between 2013-03-01 and 2013-05-20. This correlates with the announcement of the first debt exchange proposal by the Greek government (on 24 February 2012) and the aftermath of December's 2012 second default event (Moody's Investors Service 2014).

[3]Retrieved from `http://www.federalreserve.gov/datadownload/`

Chapter 5

Univariate calibration

We performed the calibration of the CGMY model parameters to the dataset by applying the `fmincon` non-linear optimization function of MATLAB® to (3.18), with suitable restrictions $C > 0$, $G > 0$, $M > 0$ and $Y < 2$. We used weekly quotes from the beginning of 2010 until the end of February of 2014, and the full structure of observed tenors $T \in \{1, 3, 5, 7, 10\}$ years (Y).

Figures 5.1 and 5.2 show that the CGMY model accurately captures the empirical features of the CDS spreads term structure throughout the time series lifecycle, for the Portuguese (PT), Irish (IE), Italian (IT) and Spanish (SP) sovereigns. The fit looses accuracy for the Greek (GR) sovereign series around the peak of its short maturity tenors (from January 2012 to July 2012), when the calibration is based on the full set of available tenors. If the calibration is restricted to the tenors $T \in \{1, 5, 10\}$ years, the accuracy improves significantly. Figure 5.3 illustrates this behavior.

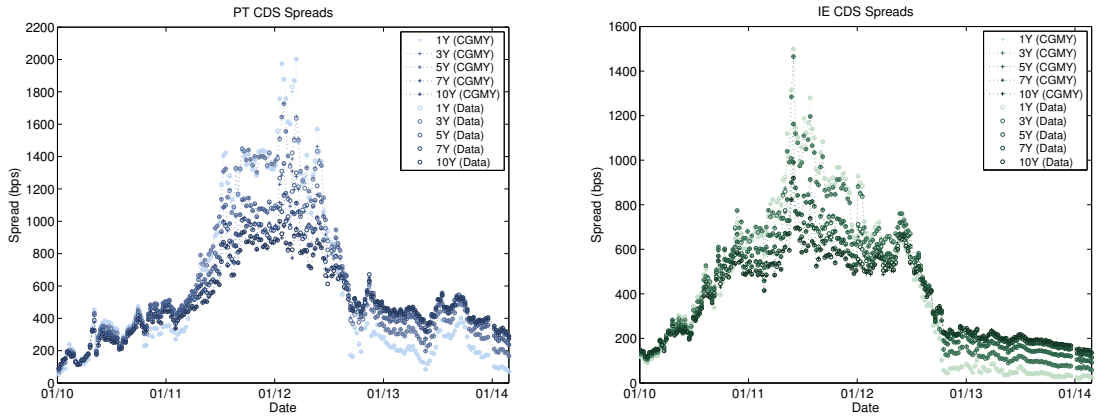

Figure 5.1: Calibration results: Portugal (PT) and Ireland (IE)

The precision of the model's fit can be assessed in Figure 5.4, displaying the distribution of the optimal absolute and relative root mean square errors (RMSE). The latter is computed as the ratio of the absolute RMSE to the average CDS spread across all tenors.

Although some outliers can be observed, especially in the series where more volatility and/or high spread values prevail, we can see that the third quartile of the relative RMSE distribution is below 1.5% for the Portuguese, Irish, Italian and Spanish sovereigns. Taking the Greek time series as a whole, only the calibration using the restricted set of tenor provides accurate enough results. Table B.1, in Appendix B.1.2, details these results by presenting key statistics of the RMSE distribution.

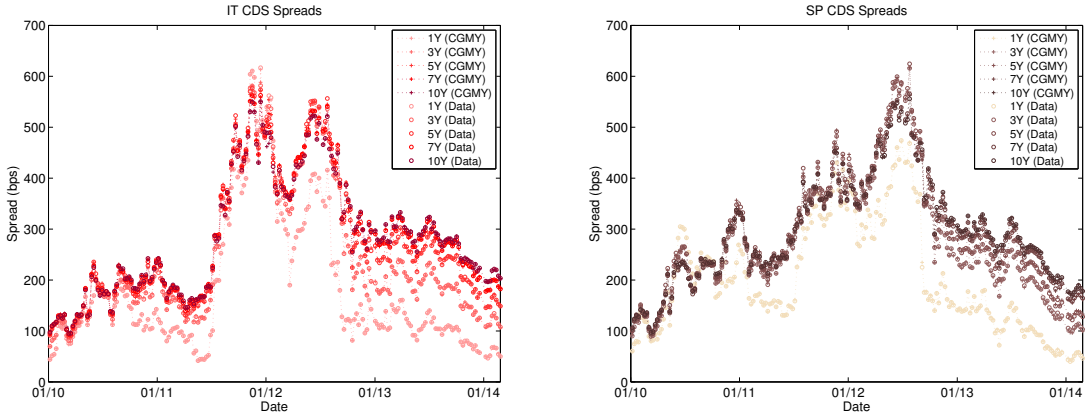

Figure 5.2: Calibration results: Italy (IT) and Spain (SP)

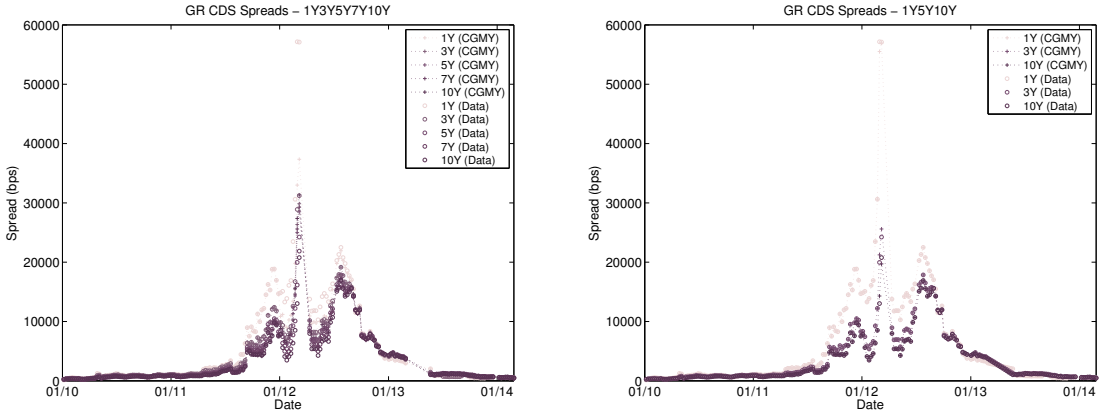

Figure 5.3: Calibration results: Greece (GR): calibration based on 1Y, 3Y, 5Y, 7Y and 10Y tenors vs. calibration based on 1Y, 5Y and 10Y tenors.

It is important to emphasize that multiple optima might be found numerically. In fact, the computational trials we performed showed that the optimization procedure is very sensitive to the starting values used: usually, several runs were required to reach accurate enough results. Furthermore, the objective function (3.18) does note cater explicitly for the stability of the calibrated parameters.

We could possibly extended it using the amendment discussed in Fang *et al.* (2010), where the regularization term

$$\gamma \cdot \|\boldsymbol{\Theta}_d - \boldsymbol{\Theta}_{d-1}\| \tag{5.1}$$

is added to the original RMSE $(\theta_1, \ldots, \theta_n)$ objective function. $\boldsymbol{\Theta}_d$ and $\boldsymbol{\Theta}_{d-1}$ are the parameter vectors for the current calibration date, d, and the previous one, $d-1$, respectively. The scalar γ needs to be empirically calibrated.

Although we have not tried to investigate the stability of the calibrated parameters, we plot their evolution over time in Appendix B.1.1 (Figures B.1 to B.5), against the backdrop of the 5-year CDS spread. It is clearly noticeable that peak periods tend to be linked with a fundamental switch in the model's properties: namely, the Y parameter drops bellow zero and so the process moves from infinite to finite activity, a behavior especially striking in the Greek series (Figure B.5). This is consistent with market conditions leading to the arrival

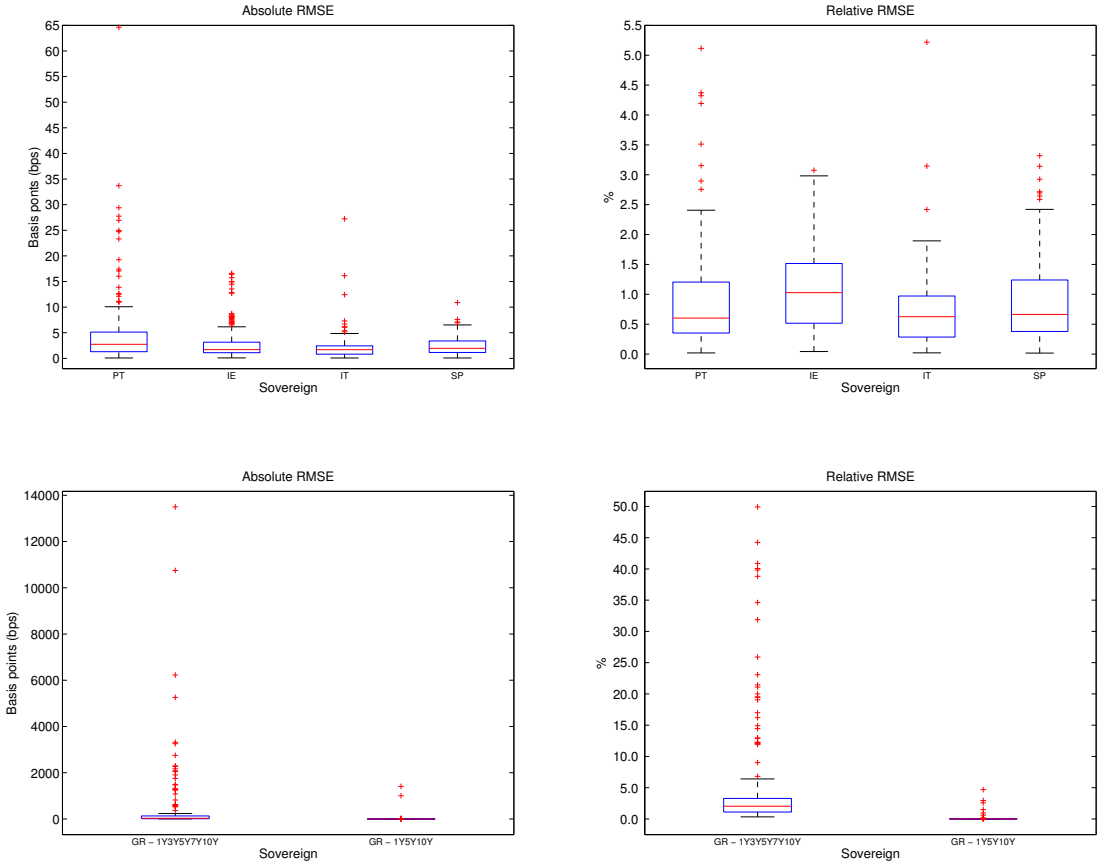

Figure 5.4: Calibration results: absolute and relative root mean square error (RMSE) distribution; the box plot displays the minimum, first quartile, median, third quartile and maximum; observations considered as outliers are marked in red.

of a few sudden, large exogenous information shocks.

The default probability term structure, computed using the COS formula for the survival probability (3.6), is shown in Figures B.6 to B.8 of Appendix B.1.3.

We can witness the reflection of the parameters instability over time on the relative lack of smoothness displayed both by the default probability term structures and the series of calibrated parameters.

In Appendix B.1.4 we compare the CGMY and the Brownian motion dynamics and illustrate the drawbacks of the latter, as previously discussed in Chapters 1 and 2.

Remark (*A note on the algorithm's performance*). Using a laptop with an Intel Core i5 2.4 GHz processor and 8 GB 1600 Mhz RAM running MATLAB® R2014a, the simultaneous computation of the calibrated model's CDS spreads for tenors $T \in \{1, 3, 5, 7, 10\}$ years and the discretization of the survival probability function for the same time points takes an average processing time of 0.54 seconds per date.

Chapter 6

Multivariate default modeling

In this chapter, we will model the latent sovereign asset value process using the Variance Gamma (VG) model[1], and take advantage of its time-changed Brownian motion representation to introduce correlation between sovereigns through a common Gamma time change component. We will illustrate this technique by performing a joint calibration from CDS market data, for an arbitrarily set date. By simulating dependent paths, we will then be able to estimate joint and conditional survival probabilities. The calibration procedure is a simple adaptation of the unidimensional COS method.

Our approach relies only on the explicit knowledge of the characteristic function (for calibration purposes) and the time change distribution (for simulation purposes). In principle, we could apply it as well to the more general CGMY model, previously used in the univariate calibration. As we have briefly mentioned in Section 2.4.2, the latter also admits a time change Brownian motion representation, albeit implicitly defined by its Laplace transform. We have opted to use the VG model in the extension of the COS method to a multidimensional setting because the simulation procedure is straightforward. Additionally, we will see that the marginal calibration is also quite accurate (although not as accurate as the one achieved with the CGMY model, at the expense of an extra parameter). The work we develop in this chapter simply aims to *illustrate* the joint calibration and simulation procedures, whereas previously we have conducted weekly marginal calibrations for an extended time period, and each of the five sovereigns under study. The simulation of the CGMY process as a time-changed Brownian motion would possibly require a numerical inversion of the Laplace transform, an avenue we have not considered pursing within the scope of this work.

6.1 Multivariate Variance Gamma model

6.1.1 Common Gamma time change

Following Cariboni and Schoutens (2009), in Section 8.4, we start by considering:

- a N-dimensional Brownian motion with drift $\mathbf{W} = \left(W_t^{(1)}, \ldots, W_t^{(N)}, t \geq 0\right)$,

$$W_t^{(i)} = \theta_i t + \sigma_i B_t^{(i)},\ \theta_i \in \mathbb{R},\ \sigma_i > 0,\ i = 1, \ldots, N,$$

  where $\mathbf{B} = \left(B_t^{(1)}, \ldots, B_t^{(N)}, t \geq 0\right)$ is a vector of (possibly) correlated standard Brownian motions, with correlation matrix $\left(\rho_{ij}^B\right)$;

[1] Described in Section 2.4.1.

- an independent, common Gamma time change $\mathbf{G} = \{G_t, t > 0\}$, with parameters $\left(\frac{1}{\nu}, \frac{1}{\nu}\right)$, $\nu > 0$.

As we have seen previously, this construction implies that the marginal processes

$$X_t^{(i)} := W_{G_t}^{(i)} = \theta_i G_t + \sigma_i B_{G_t} \tag{6.1}$$

are Variance Gamma distributed with parameters $(\sigma_i, \nu, \theta_i)$. Parameters σ_i and θ_i are idiosyncratic to each marginal process (respectively, its volatility and drift), while the common parameter ν defines the single Gamma time change. The embedded dependency structure has two different sources: the correlation between the Brownian motions and the common time change. The latter is crucial to the construction, as it ensures that the marginal processes' jumps occur simultaneously.

We can calibrate the parameters ν, σ_i and θ_i, $i = 1, \ldots, N$, by applying the COS method to N Variance Gamma characteristic functions of the form (2.5), with a common ν parameter, and then minimizing the root mean square error (RMSE) of the CDS spreads across all sovereigns.

The correlation coefficients between components are computable in the time unit as

$$\rho_{ij} = \frac{\mathbb{E}\left[X_1^{(i)} X_1^{(j)}\right] - \mathbb{E}\left[X_1^{(i)}\right]\mathbb{E}\left[X_1^{(j)}\right]}{\sqrt{\mathbb{V}\left[X_1^{(i)}\right]}\sqrt{\mathbb{V}\left[X_1^{(j)}\right]}} = \frac{\theta_i\theta_j\nu + \sigma_i\sigma_j\rho_{ij}^B}{\sqrt{\sigma_i^2 + \theta_i^2\nu}\sqrt{\sigma_j^2 + \theta_j^2\nu}}. \tag{6.2}$$

This relationship allows us to solve for the correlation coefficients between the standard Brownian motions, ρ_{ij}^B, from previously known (or estimated) correlation coefficients between the asset value processes, ρ_{ij}.

The simulation procedure would then run as follows:

Step 1 Perform a joint calibration of parameters $(\sigma_i, \nu, \theta_i)$ on market CDS spreads data;

Step 2 Estimate (or define) the correlation matrix (ρ_{ij}) between the marginal asset value processes $X_t^{(i)}$;

Step 3 Compute the Brownian motion correlation matrix $\left(\rho_{ij}^B\right)$ from (6.2);

Step 4 Jointly simulate dependent paths of the marginal processes using the characterization of the VG process as a time-changed Brownian motion.

Although empirical estimation of the correlation between the latent asset value processes could be implemented[2], we have elected to use as sole dependency source the common time change.[3] Consequently, we will skip step 2 of the simulation procedure and use the identity matrix in step 3 (implied by independent marginal Brownian motions).

[2]Let us consider the independent increments $\varepsilon := X_{t+\Delta t} - X_t$. In the Variance Gamma model, the distribution of ε is known, as there is a closed formula for its density, involving modified Bessel functions of the third kind (Cariboni and Schoutens 2009). In other models, such as the CGMY, where the distribution of the increments is not explicitly know, we could resort to the COS transition density approximation formula (3.2). The correlation between increments could then be empirically estimated from the relationship

$$X_{t+\Delta t} - X_t = F_\varepsilon^{-1}\left(P(t + \Delta t, t + \Delta t + T)\right) - F_\varepsilon^{-1}\left(P(t, t + T)\right),$$

where $P(t, t+T) = \mathbb{P}\left(X_{t+T} \leq \ln R\right)$ is the survival probability in $(t, t+T)$, i.e., the survival probability for tenor T at time t, and F_ε is the distribution function of the random variable ε.

[3]An approach supported by empirical tests where correlation was introduced only in the multivariate Brownian motion process: the simulation results have shown no conclusive evidence of dependency on the estimated joint and conditional default probabilities.

Calibration results

As our purpose is simply to illustrate the application of the multivariate VG model, we will work with a single, arbitrarily chosen date (2014-02-26, the same we use to compare the CGMY process with the Brownian motion in Appendix B.1.4).

We start by calibrating the multidimensional, common time change VG model using the full set of available CDS spreads (all 5 tenors – 1, 3, 5, 7 and 10 years – and all 5 sovereigns).

Figure 6.1 displays the CDS spreads implied by the multidimensional VG model against the market data, as well as the survival probabilities. We can witness an overpricing trend on the lower tenors (1 and 3 years) and an underpricing one on the higher tenors (7 and 10 years), for all sovereigns except Greece (GR). This behavior is especially clear in the case of the Portuguese (PT) sovereign.

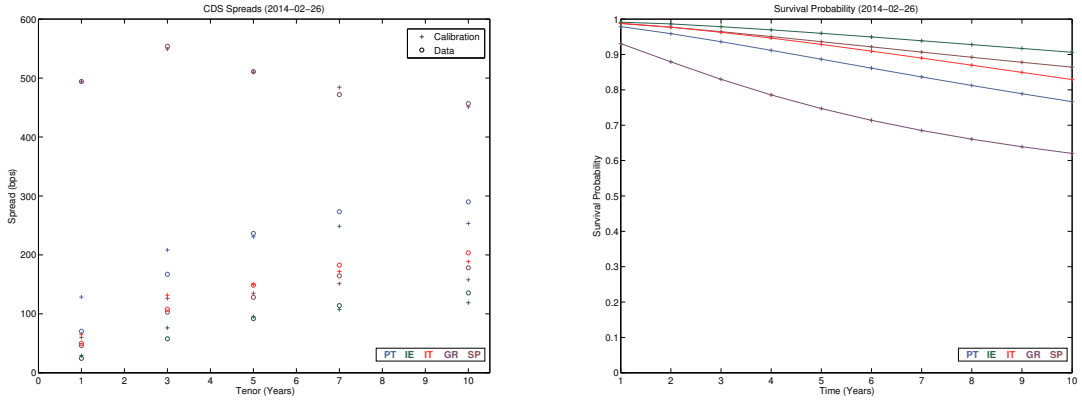

Figure 6.1: Joint calibration of PT, IT, IE, GR and SP spreads, and implicit survival probabilities. Calibration is achieved with an optimal RMSE of 20.46 basis points, comparing with an average RMSE of 6.04 for the corresponding marginal calibrations. In relative terms, these figures are 9.72% and 4.23%, respectively.

The calibration accuracy improves significantly (from 20.46 to 5.08 basis points) when we restrict it to the 3 sovereigns with lower and more homogeneous CDS spreads, namely Ireland (IE), Italy (IT) and Spain (SP). Figure 6.2 highlights this observation.

These results suggest that we could improve the fit by adding idiosyncratic, Gamma distributed components to the time change for the remaining two sovereigns (PT and GR). Their calibration would then be conditional on an optimal, common time change component, previously obtained from the set of sovereigns whose CDS spreads are considered sufficiently homogeneous (in our case, IE, IT and SP). The next section clarifies this procedure.

6.1.2 Gamma time change with common and idiosyncratic components

Given a common Gamma time change component, G_t, we introduce an additional *independent* idiosyncratic component, $G_t^{(i)}$, also Gamma distributed, with parameters $\left(\frac{1}{\nu_i}, \frac{1}{\nu_i}\right)$, i.e., such that $G_1^{(i)} \sim \Gamma\left(\frac{1}{\nu_i}, \frac{1}{\nu_i}\right)$. We then set the full time change for sovereign i as

$$H_t^{(i)} := \alpha_i G_t + (1-\alpha_i) G_t^{(i)},\ \alpha_i \in (0,1). \tag{6.3}$$

We can interpret the common and idiosyncratic time change components as proxies for systematic and specific credit risk factors.

The previous definition implies that

$$\mathbb{E}\left[H_1^{(i)}\right] = \alpha_i \mathbb{E}\left[G_1\right] + (1-\alpha_i)\mathbb{E}\left[G_1^{(i)}\right] = 1 \Rightarrow \mathbb{E}\left[H_t^{(i)}\right] = t,$$

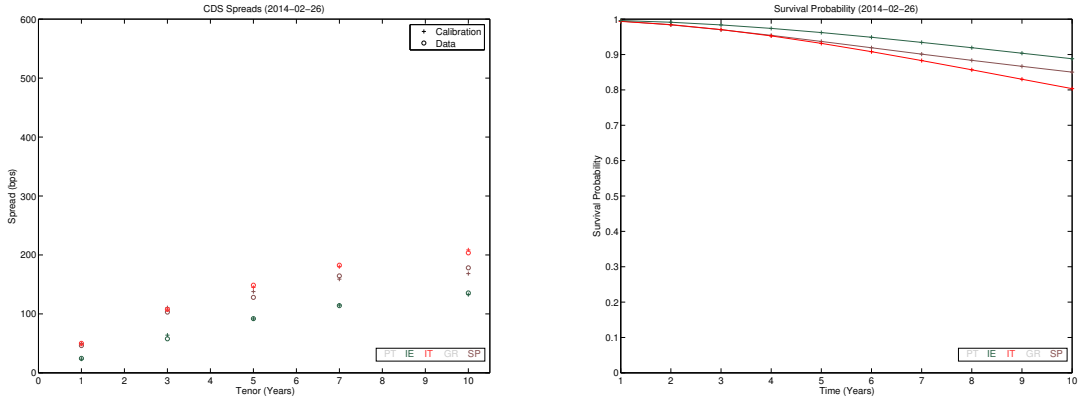

Figure 6.2: Joint calibration of IE, IT and SP spreads, and implicit survival probabilities. Calibration is achieved with an optimal RMSE of 5.08 basis points, comparing with an average RMSE of 6.59 for the corresponding marginal calibrations. In relative terms, these figures are 4.39% and 5.98%, respectively.

thereby preserving the time change invariance property (2.6). Furthermore, under our construction all three sources of randomness, G_t, $G_t^{(i)}$ and $B_t^{(i)}$ are independent. With this assumption in mind, we can easily obtain the characteristic function of the time change:

$$\phi_{H_t^{(i)}}(\omega) = \left[\phi_{H_1^{(i)}}(\omega)\right]^t,$$

where

$$\phi_{H_1^{(i)}}(\omega) = \phi_{G_1}(\alpha_i\omega) \cdot \phi_{G_1^{(i)}}\left((1-\alpha_i)\omega\right).$$

As a consequence, the multivariate process with marginals

$$X_t^{(i)} := W^{(i)}_{H_t^{(i)}} = \theta_i H_t^{(i)} + \sigma_i B_{H_t^{(i)}} \tag{6.4}$$

is also infinitely divisible.

Following the reasoning of Section 2.4.1, the characteristic function of the marginal processes will be given by

$$\phi_{X_t^{(i)}}(\omega) = \left[\phi_{X_1^{(i)}}(\omega)\right]^t,$$

with

$$\phi_{X_1^{(i)}}(\omega) = \phi_{H_1^{(i)}}\left(\theta_i\omega + \frac{1}{2}i\sigma_i^2\omega^2\right) = \left[1 - i\alpha_i\nu\left(\theta_i\omega + \frac{1}{2}i\sigma_i^2\omega^2\right)\right]^{-\frac{1}{\nu}} \cdot \left[1 - i(1-\alpha_i)\nu_i\left(\theta_i\omega + \frac{1}{2}i\sigma_i^2\omega^2\right)\right]^{-\frac{1}{\nu_i}}. \tag{6.5}$$

The calibration of the multivariate VG model with common *and* idiosyncratic Gamma time change components can then be described as follows:

Step 1 Calibrate the multidimensional VG model with a common time change from a homogeneous CDS spreads dataset, following the procedure detailed in Section 6.1.1. We will then obtain parameters $(\sigma_i, \nu, \theta_i)$ for $i \in \mathcal{S}_C$, the set of "homogeneous" sovereigns. This will provide a common Gamma time change component, defined by parameters $\left(\frac{1}{\nu}, \frac{1}{\nu}\right)$, to use in the following step;

Step 2 Calibrate the remaining sovereigns by applying the COS method to the marginal processes (6.4), whose characteristic functions are given by (6.5). We will then obtain parameters $(\sigma_i, \theta_i, \alpha_i)$ for $i \in \mathcal{S}_I$, the set of sovereigns whose value processes are modeled with the inclusion of an idiosyncratic time change component.

In our case, step 1 means we calibrate the multidimensional VG model with a common time change G_t for sovereigns $i \in \mathcal{S}_C = \{\text{IE, IT, SP}\}$. In step 2 we calibrate the remaining sovereigns $i \in \mathcal{S}_I = \{\text{PT, GR}\}$. For this, we weigh the common time change component component previously obtained, G_t, with the idiosyncratic time change component, $G_t^{(i)}$, according to (6.3). So, given a calibration of parameters $(\sigma_i, \nu, \theta_i)_{i\in\{\text{IE,IE,SP}\}}$, we reapply the COS framework to (6.5) to calibrate the remaining parameters $(\sigma_i, \theta_i, \alpha_i)_{i\in\{\text{PT,GR}\}}$.

Calibration results

Figure 6.3 presents the calibration of the multivariate VG model with common and idiosyncratic Gamma time change components, for the dataset used in the previous section. By introducing an idiosyncratic component in the time change of the sovereigns with higher CDS spreads (PT and GR), we improve the global accuracy of the fit from 20.46 to 10.28 basis points. For comparison purposes, we have also performed the marginal calibration of the univariate VG model, for all sovereigns. The calibration accuracy, measured as relative RMSE, has proven similar between both calibration procedures (4.89% for the multivariate calibration vs. an average of 4.23% for the marginal, univariate calibrations). We observe no significant qualitative difference between the survival probability functions.

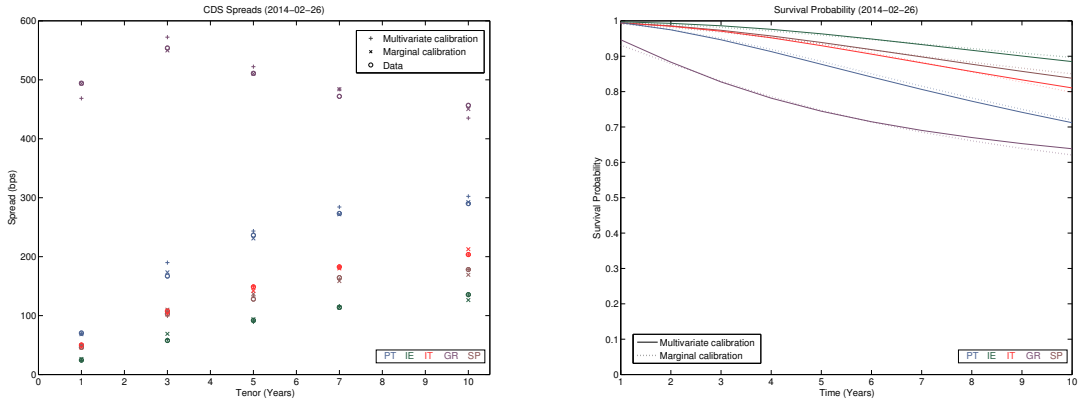

Figure 6.3: Joint calibration of IT, IE and SP CDS spreads and conditional idiosyncratic calibration of PT and GR CDS spreads; implicit survival probabilities. Calibration is achieved with an optimal RMSE of 10.28 basis points (4.89% in relative terms).

Table B.4, in Appendix B.2.1, sums up the calibration results discussed in this and the previous sections.

6.2 Estimation of joint and conditional default probabilities

Having achieved a joint calibration of the multivariate Variance Gamma model (possibly with the inclusion of idiosyncratic components on the time change, as described in the previous section), we can capitalize on the time-changed Brownian motion representation (6.4) to simulate joint, correlated paths without difficulty. All we need is to take independent random

draws from the standard Normal and the Gamma[4] distributions. Appendix C presents a detailed description of the simulation procedure.

Using the calibrated parameters for the multivariate Variance Gamma model with idiosyncratic components for sovereigns PT and GR (cf. Table B.4 in Appendix B.2.1, scenario $i = 8$), we have simulated 100 000 correlated paths and estimated the joint and conditional default probabilities up to $T = 1, 5, 10$ years, respectively

$$\mathbb{P}\left(\min_{0\le t\le T} X_t^{(i)} < \ln R,\ \min_{0\le t\le T} X_t^{(j)} < \ln R\right) \text{ and } \mathbb{P}\left(\min_{0\le t\le T} X_t^{(i)} < \ln R \,\middle|\, \min_{0\le t\le T} X_T^{(j)} < \ln R\right).$$

Figure 6.4 depicts one such simulation, clearly illustrating the simultaneous nature of the jumps when a common time change is used (i.e., for sovereigns IT, IE and SP), and the joint default of PT and GR within 10 years.

Tables B.5 and B.6, in Appendix B.2.2, present the estimated default probabilities for the reference date 2014-02-26. For comparison purposes, marginal default probabilities are also provided. The estimated conditional default probabilities show a clear dependency between defaults.

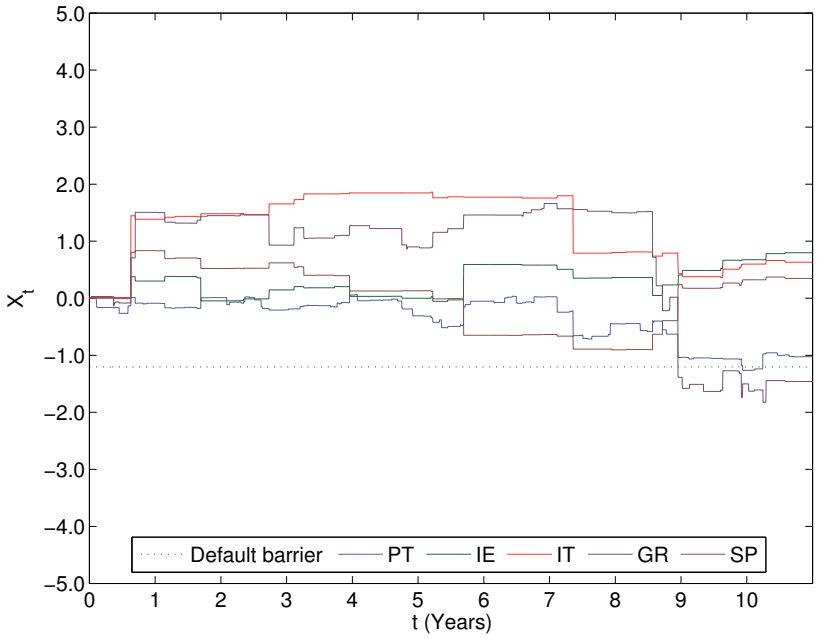

Figure 6.4: Multivariate VG model: a joint simulation of paths for reference date 2012-02-26. The default barrier is set with recovery rate $R = 0.3$ for all sovereigns. For each of three monitored time periods T (1, 5 and 10 years), a sovereign default is registered if the simulated path crosses the default barrier $h \equiv \ln R$ up to time T. Default events are observable for sovereigns GR and PT, just before 9 and 10 years, respectively. On a laptop with an Intel Core i5 2.4 GHz processor and 8 GB 1600 Mhz RAM running MATLAB® R2014a, each batch of 1000 simulations takes an average time of 4.42 seconds.

[4]With parameters $\left(\frac{1}{\nu}, \frac{1}{\nu}\right)$ and $\left(\frac{1}{\nu_i}, \frac{1}{\nu_i}\right)$, for the common ($G_1$) and idiosyncratic ($G_1^{(i)}$) components of the time change $H_1^{(i)}$.

Chapter 7

Conclusions

In this work we have calibrated the Lévy CGMY model to selected Euro area CDS spreads using the Fourier-cosine series expansion method of Fang *et al.* (2010), from which the default probability term structure could then be inferred at no further computational cost.

The calibration procedure was implemented using the non-linear, constrained optimization MATLAB® function `fmincon`. It has displayed a significant degree of sensitivity to initial conditions, as would be foreseeable given the nature of the numerical optimization problem. Empirical evidence has shown that several local optima were reachable. On occasion, this has forced us to run the calibration algorithm a number of times before attaining optima whose accuracy matched the one of previous dates, especially under distress circumstances. As a consequence, some of the optima found might not suitably approximate *the* optimal solutions, given the constrained parameter space. Notwithstanding this caveat, the univariate calibration results have proven able to accurately reproduce the CDS market data and adequately capture the different stages in its lifecycle.

The evolution of the calibrated parameters over time – depicted in Figures B.1 to B.5 of the appendix – provides some empirical insights into the nature of the underlying latent asset value process, of which we emphasize the following:

- The C parameter, correlating with the global level of activity of the process (and so its kurtosis), tends to move in tandem with the most liquid, 5 year CDS spread;
- Parameters G and M, controlling the skewness of the process increments, tend to move in opposite directions whenever the CDS term structure is inverted, i.e., when the short term spreads cross the value of the long term ones and we reach a stage where the CDS spreads tend to *increase* with the *decrease* of the tenor;
- The Y parameter controls the behavior of the Lévy measure near zero, and so the nature of the very small jumps. It allows to easily infer the process activity and variation regimes. We could describe the data behavior with a qualitative rule of thumb: stable periods (characterized by sustained low volatility, moderate historical spread values and no inversion effect on the CDS spreads term structure) lead to a an infinite variation, infinite activity regime ($1 < Y < 2$), where the jumps governing the process would be mostly endogenous and "smooth"; the onset of a distress period moves the process to a finite variation, but still infinite activity regime ($0 < Y < 1$); and the full setting of distress conditions induces finite activity ($Y < 0$). This is intuitive, as under the latter circumstances we can expect the arrival of sudden, exogenous shocks. These shocks convey the notion that the market has incorporated new pieces of relevant information about the credit riskiness of the underlying obligors.

Figures B.1 to B.5 also clearly show that stress conditions displayed by the CDS spread market data are prone to render the calibration unstable. We could tackle this hurdle by introducing a stability penalization term in the optimization objective function, such as the one suggested in (5.1). A sensitivity analysis of the implied CDS spreads on the model parameters could achieve an adequate calibration of the parameter γ.

We have hinted at the computational efficiency of the COS method in Chapter 5. This assessment could be further enhanced by comparing the average computation times we have measured with the ones from other well established (barrier) option pricing techniques. A benchmark method for this purpose is the Fourier transform inversion method using the FFT, as introduced by Carr, Chang and Madan (1998) and applied to CDS pricing by Cariboni and Schoutens (2008).

A secondary objective of this work was the illustration of a possible extension of the univariate COS methodology to a multidimensional calibration setting, introducing dependency between sovereigns. To this effect, we have resorted to the representation of the Variance Gamma (VG) model (a particular instance of the CGMY model, with parameter $Y = 0$) as a time-changed Brownian motion and modified the Gamma time change by adding an idiosyncratic component to a common, systematic one. The MATLAB® code developed for the univariate calibration could then be reused with minimal changes. Using this representation, the simulation of dependent paths was straightforward and computationally efficient, as was the estimation of joint and conditional default probabilities. Arguably, we could extend the multivariate approach to the CGMY model through its time-changed Brownian motion representation (Madan and Yor, 2008).

Our empirical work showed that adding dependency solely by correlating the underlying Brownian motions did not reflect in any significant way either in the joint or the conditional default probabilities. To break the (near) independent probabilities pattern, the simultaneous jumps introduced by taking a *common* time change component were crucial.[1] The results have also proven that the multidimensional calibration displayed a similar degree of accuracy to the one of the marginal VG calibrations, with the added benefit of introducing a dependency structure.

Further work avenues could address the analysis of the joint and conditional probability structure over time. This would require applying both the joint calibration and simulation procedures to our full dataset. Results could then be used to measure default contagion. Suppose we are interested in assessing the impact of a default event for a specific sovereign i. Then, for each sovereign $j \neq i$, we could consider the difference between the probability that j defaults given that i defaults, and the probability that j defaults given that i *does not* default. This would be a simple and intuitive proxy for default contagion.

We could also enhance the methodology by considering other Euro area sovereigns. However, we must recognize that some practical implementation issues would forcibly arise. First, we expect the increase in the calibration procedure's complexity to require a significant extra amount of running time. Secondly, as the computation of joint and conditional default probabilities relies on a joint simulation of *paths*, we expect our methodology to become burdensome when we start increasing the number of sovereigns. Thirdly, several *ad hoc* modeling assumptions would have to be made (namely, the choice of sovereigns for which an explicit idiosyncratic component would be introduced). We must emphasize that the practical application of this approach to higher dimension problems (such as measuring the credit risk of a portfolio) is necessarily limited.

[1] We can confront this with the well studied behavior of intensity based diffusion models, where even perfectly correlated intensities are not enough to capture significant default correlation levels. Jump-diffusion models considering simultaneous intensity jumps overcome this obstacle. We can intuitively compare the intensity to the time change in our structural approach.

Appendix A

Auxiliary proofs

A.1 Proof of Proposition 3.1

Proof. For $f : [0, \pi] \to \mathbb{R}$, the Fourier-cosine series reads

$$f(\theta) = \sum_{k=0}^{+\infty}{}' A_k \cos(k\theta),$$

with the Fourier-cosine coefficients given by

$$A_k = \frac{2}{\pi} \int_0^\pi f(\theta) \cos(k\theta) d\theta.$$

We start by considering a probability density function f with support $\operatorname{supp} f = [a, b]$. We can write its Fourier-cosine series expansion from the previous expressions performing the linear change of variables $\theta = \frac{x-a}{b-a}\pi$:

$$f(x) = \sum_{k=0}^{+\infty}{}' A_k \cos\left(k\pi \frac{x-a}{b-a}\right) \tag{A.1}$$

$$A_k = \frac{2}{b-a} \int_a^b f(x) \cos\left(k\pi \frac{x-a}{b-a}\right) d\theta. \tag{A.2}$$

Let us approximate the corresponding characteristic function ϕ by truncating the Fourier integral (2.1) to $[a, b]$:

$$\phi_1(\omega) := \int_a^b e^{i\omega x} f(x) dx \simeq \int_{\mathbb{R}} e^{i\omega x} f(x) dx = \phi(\omega). \tag{A.3}$$

Now,

$$\phi_1\left(\frac{k\pi}{b-a}\right) = \int_a^b e^{ik\pi \frac{x}{b-a}} f(x) dx,$$

and so

$$\int_a^b e^{ik\pi \frac{x-a}{b-a}} f(x) dx = \phi_1\left(\frac{k\pi}{b-a}\right) e^{-ik\pi \frac{a}{b-a}}. \tag{A.4}$$

Comparing $(A.2)$ and $(A.4)$, we get the following approximation for the Fourier coefficients:

$$A_k \simeq \frac{2}{b-a} \operatorname{Re}\left\{\phi\left(\frac{k\pi}{b-a}\right) e^{-ik\pi \frac{a}{b-a}}\right\}. \tag{A.5}$$

We now consider the transition density $f(y|x) \equiv f_{X_t|X_s}(y|x)$ and rewrite $(A.1)$ and $(A.2)$ as

$$f(y|x) = \sum_{k=0}^{+\infty}{}' A_k(x) \cos\left(k\pi \frac{y-a}{b-a}\right)$$
$$A_k(x) = \frac{2}{b-a}\int_a^b f(y|x)\cos\left(k\pi\frac{y-a}{b-a}\right) d\theta.$$

The conditional characteristic function can be written as

$$\begin{aligned}\phi(\omega|x) &= \int_{\mathbb{R}} e^{i\omega y} f(y|x) dy \\ &= e^{i\omega x}\int_{\mathbb{R}} e^{i\omega(y-x)} f(y|x) dy \\ &= e^{i\omega x}\int_{\mathbb{R}} e^{i\omega z} f(z+x|x) dz \\ &= e^{i\omega x}\phi(\omega|0),\end{aligned}$$

by independence and stationarity of increments. The approximation for the Fourier coefficients $(A.5)$ then becomes

$$\begin{aligned}A_k(x) &\simeq \frac{2}{b-a}\mathrm{Re}\left\{\phi\left(\frac{k\pi}{b-a}; x\right) e^{-ik\pi\frac{a}{b-a}}\right\} \\ &= \frac{2}{b-a}\mathrm{Re}\left\{\phi\left(\frac{k\pi}{b-a}; 0\right) e^{ik\pi\frac{x-a}{b-a}}\right\} \\ &= \frac{2}{b-a}\mathrm{Re}\left\{\phi_{X_{t-s}}\left(\frac{k\pi}{b-a}\right) e^{ik\pi\frac{x-a}{b-a}}\right\} \\ &= \frac{2}{b-a}\mathrm{Re}\left\{\varphi_{levy}\left(\frac{k\pi}{b-a}, t-s\right) e^{ik\pi\frac{x-a}{b-a}}\right\},\end{aligned}$$

and we obtain the COS formula to approximate the transition density:

$$f_{X_t|X_s}(y|x) = \frac{2}{b-a}\sum_{k=0}^{N-1}{}'\mathrm{Re}\left\{\varphi_{levy}\left(\frac{k\pi}{b-a}, t-s\right) e^{ik\pi\frac{x-a}{b-a}}\right\} \cdot \cos\left(k\pi\frac{y-a}{b-a}\right) + \varepsilon_f. \quad (A.6)$$

□

Remark (*The error term* ε_f). As previously mentioned, two different causes contribute to the error term ε_f.

First, the support of the transition density $f_{X_t|X_s}(y|x)$ is truncated to $[a, b]$ in $(A.3)$ to approximate the process characteristic function. As the condition for the existence of the Fourier transform implies that the integrand decays rapidly to 0 as $x \to \pm\infty$, a and b can be suitably chosen to control this approximation error.

Secondly, we only consider the first N terms of the Fourier-cosine series expansion, but the convergence of the series is fast enough for the error term due to this cause to be small.

A.2 Proof of Proposition 3.2

Proof. Let us start by once more truncating the integration domain:

$$p(x, t_m) = \int_h^b f_{X_{t_{m+1}}|X_{t_m}}(y|x) p(y, t_{m+1})\, dy + \varepsilon_p.$$

Plugging the transition density formula $(A.6)$ in the previous expression, we get

$$p\left(x,t_m\right) = \sum_{k=0}^{N-1}{}' \underbrace{\mathrm{Re}\left\{\varphi_{levy}\left(\frac{k\pi}{b-a},\Delta t\right)e^{ik\pi\frac{x-a}{b-a}}\right\}}_{\phi_k(x)} \cdot \\ \cdot \underbrace{\frac{2}{b-a}\int_h^b \cos\left(k\pi\frac{y-a}{b-a}\right)p\left(y,t_{m+1}\right)dy}_{P_k(t_{m+1})} + \varepsilon_{COS}$$

and so we can approximate $p\left(x,t_0\right)$ by

$$p(x,t_0) = \sum_{k=0}^{N-1}{}' \phi_k(x)P_k(t_1),$$

where the final error term ε_{COS} includes ε_p, i.e., both the integral and the Fourier series truncation effects. The survival probability is then simply the previous expression, evaluated at $x = 0$:

$$P_{surv}(\tau) = \sum_{k=0}^{N-1}{}' \phi_k(0)P_k(t_1).$$

□

A.3 Proof of Proposition 3.5

Proof. To price the CDS contract, we take the present values of both the premium payments (premium leg) and the payment made in case of default (loss leg):

$$PV_{premium\ leg} = cN\int_0^T D(0,s)P_{surv}(s)ds$$
$$PV_{loss\ leg} = (1-R)N\int_0^T D(0,s)P_{surv}(s)\mu_s ds.$$

$D(0,t)$ is the discount factor, $P_{surv}(t)$ is the survival probability in $(0,t)$ and

$$\mu_t := -\frac{d}{dt}\ln P_{surv}(t) = -\frac{\frac{d}{dt}P_{surv}(t)}{P_{surv}(t)} \tag{A.7}$$

is the hazard rate function.[1] We should note that the term $P_{surv}(t)\mu_t$ in the integrand is simply the default density $\frac{d}{dt}P_{def}(t) = -\frac{d}{dt}P_{surv}(t)$, where $P_{def}(t) = 1 - P_{surv}(t)$ denotes the default probability up to time t.

The fair spread of the CDS contract is the spread c^* that makes both legs equal, i.e.

$$c^* = (1-R)\frac{\int_0^T D(0,s)P_{surv}(s)\mu_s ds}{\int_0^T D(0,s)P_{surv}(s)ds}. \tag{A.8}$$

Using $D(0,t) = e^{-rt}$ and $(A.7)$, we can integrate by parts

$$\int_0^T e^{-rs}dP_{surv}(t) = \left[e^{-rt}P_{surv}(t)\right]_0^T + r\int_0^T e^{-rs}P_{surv}(s)ds \\ = e^{-rT}P_{surv}(T) - 1 + r\int_0^T e^{-rs}P_{surv}(s)ds$$

[1] Also called force of mortality.

to rewrite the fair spread formula $(A.8)$ as

$$c^* = (1-R)\left[\frac{1-e^{-rT}P_{surv}(T)}{\int_0^T e^{-rs}P_{surv}(s)ds} - r\right]. \tag{A.9}$$

Approximating the integral in the denominator using the trapezoidal rule

$$\int_0^T e^{-rs}P_{surv}(s)ds \simeq \sum_{j=0}^{J} w_j e^{-r\tilde{t}_j}P_{surv}\left(\tilde{t}_j\right)\cdot\Delta t,$$

with weights

$$w_j = \begin{cases} \frac{1}{2} & j = 0, J \\ 1 & j \neq 0, J, \end{cases}$$

$(A.9)$ becomes

$$c^* = (1-R)\left[\frac{1-e^{-rT}P_{surv}(T)}{\sum_{j=0}^{J} w_j e^{-r\tilde{t}_j}P_{surv}\left(\tilde{t}_j\right)\cdot\Delta t} - r\right] + \varepsilon_c,$$

where ε_c is the error term from the integral approximation. □

Appendix B

Calibration results

B.1 Univariate CGMY calibration

B.1.1 Parameters

This section presents the evolution over time of the calibrated parameters for the CGMY model. Unless otherwise stated, all results pertain to tenors $T \in \{1, 3, 5, 7, 10\}$ years. For comparison purposes, the time series of the most liquid CDS tenor (5 years) is also shown. Some outliers were omitted.

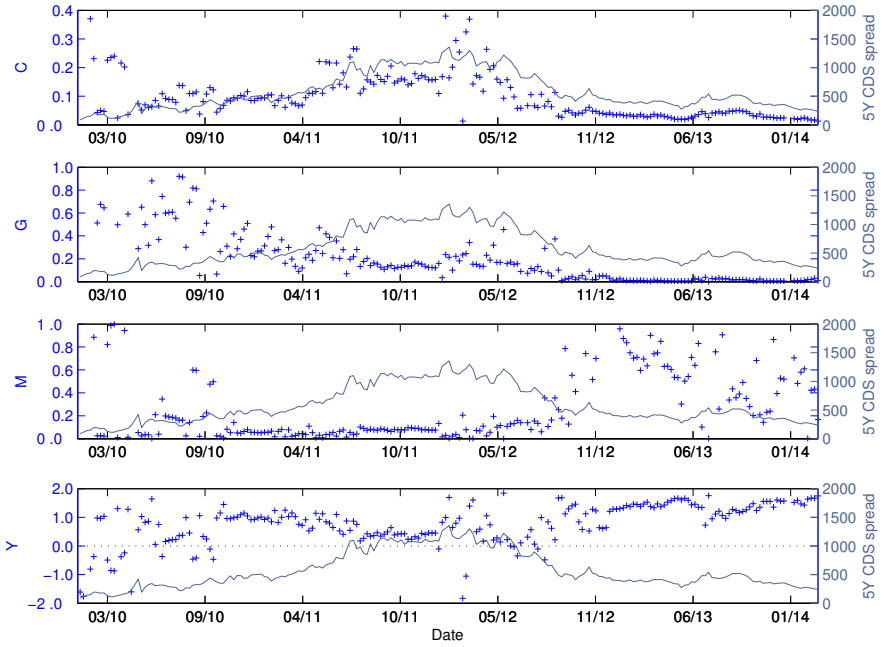

Figure B.1: Calibrated parameters for the CGMY model: Portugal (PT)

Figure B.1 presents the calibrated parameters for the Portuguese sovereign and distinctly illustrates the general conclusions previously drawn.

We start by noticing that the most liquid, 5 years CDS spread provides a yardstick for the global level of activity of the process (measured by the C parameter); furthermore, we see that sharp increases in its level lead to parameter instability.

Contrasting the series for parameters G and M with the dataset for Portugal (Figure 4.1),

we can confirm the empirical relationship between the process skewness and the "inversion" of the CDS spreads term structure. Indeed, within the calibration time frame, the period where the CDS spreads clearly *increase* with the tenor (from January to September 2012) is roughly linked to the period where $G > M$ (positive skewness); likewise, the *increase* of the CDS spreads with the tenor correlates with $G < M$ (negative skewness).

The Y parameter mimics the stable behavior of parameter C for moderate levels of the 5 year CDS spread (for example, from October 2012 onward), with values within the infinite activity, infinite variation range ($1 < Y < 2$). Notwithstanding, prevailing market conditions from mid 2011 up to October 2012 led to stressed values of the CDS spread level, and we can discern a clear switch to the infinite activity, finite variation regime ($0 < Y < 1$), yet with occasional values within the finite activity, finite variation range ($Y < 0$).

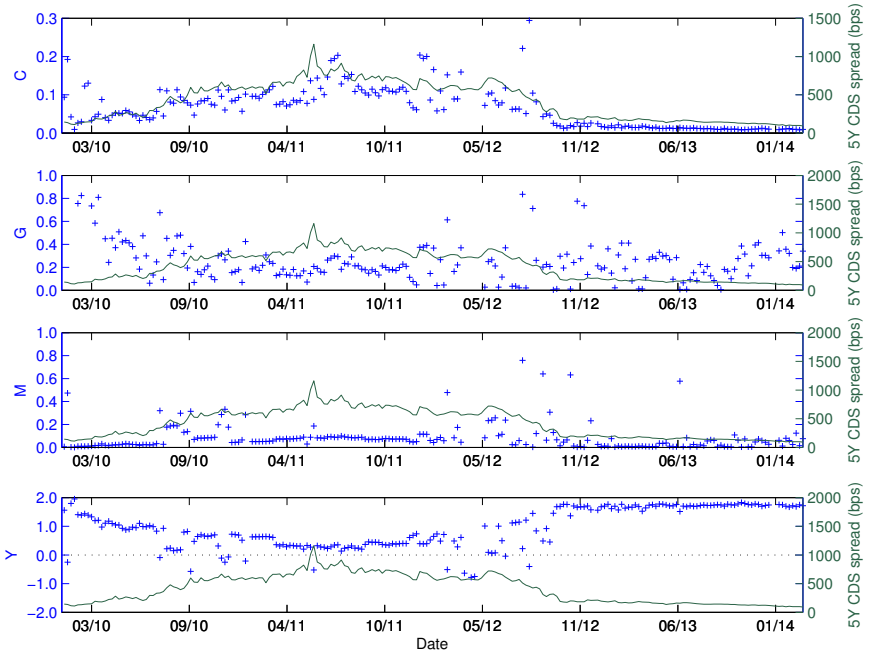

Figure B.2: Calibrated parameters for the CGMY model: Ireland (IE)

In Chapter 4, we noticed that the CDS spreads term structure for the Irish sovereign behaved quite similarity to the Portuguese one, albeit with a distinct time lag and a less pronounced peak. This is consistent with a qualitative behavior of parameters C and Y that does not deviate significantly from the one previously described for the Portuguese sovereign. Small differences are discernible, however. Figure B.2 shows that parameters G and M are approximately equal from January to September 2012, suggesting a symmetric distribution of increments that matches a near flat term structure. From that point on, the CDS spreads increase with the tenor and we revert to positive skewness ($G > M$).

Results for the Italian and Spanish data series, presented in Figures B.3 and B.4, vouch for a general increase in the stability of the C and Y parameters, stemming for comparatively moderate values of CDS spreads. However, we should note that the calibration results for Spain clearly display a sudden regime change between May and July of 2012: some of the older dates lead to $Y < 0$ (finite activity), while on the remaining $0 < Y < 1$ (infinite activity but finite variation). This coincides with a sharp decrease in the spread values, that nearly halve between June and August of 2012 (cf. Figure 4.2), and can then be a reflection of a large exogenous shock to the sovereign "value" process.

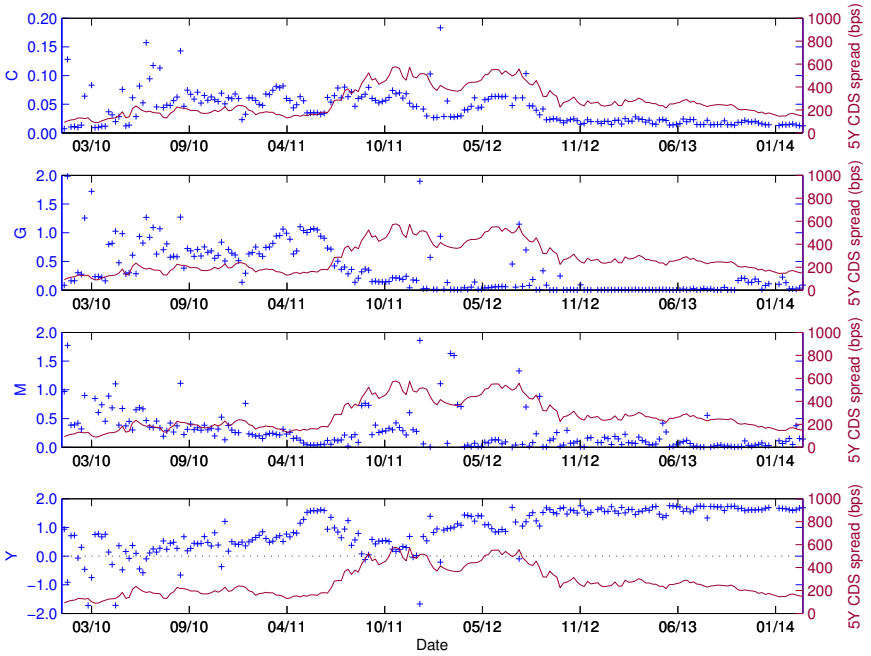

Figure B.3: Calibrated parameters for the CGMY model: Italy (IT)

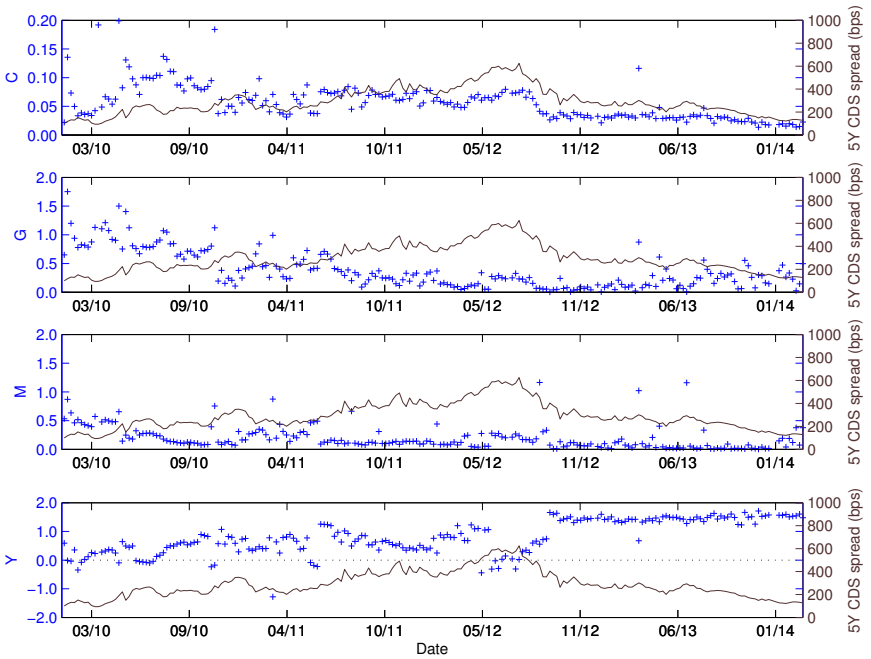

Figure B.4: Calibrated parameters for the CGMY model: Spain (SP)

Concerning the calibration results for Greece, it is worthwhile mentioning that, in accordance with previous insights, the distress period spanning October 2011 to August 2012 seemingly concurs with an extended finite variation regime. As foreseeable, given the nature of the CDS data, the Greek series leads to the most unstable calibration, even though clear trends can be observed on the C and Y time series.

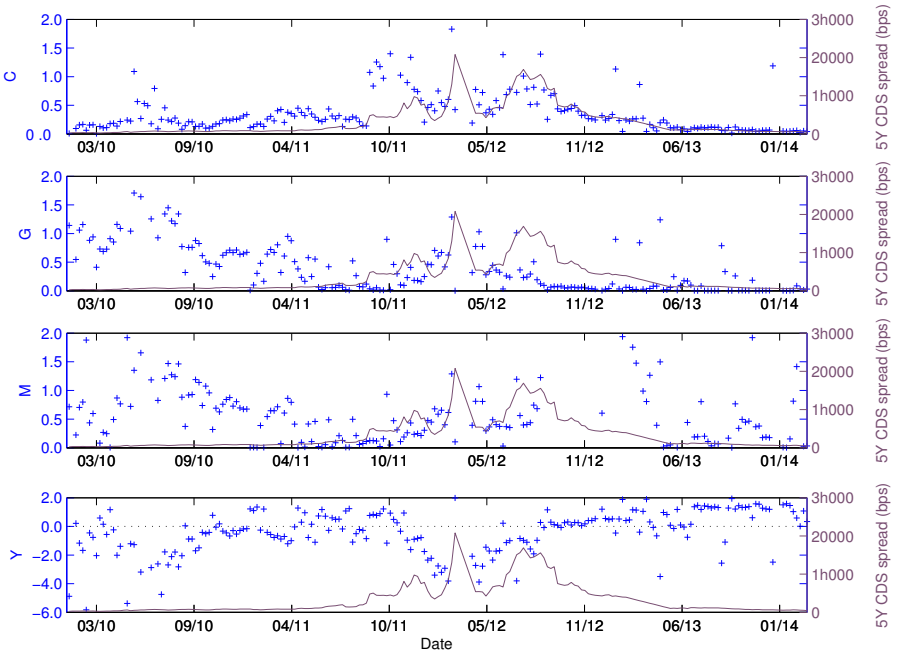

Figure B.5: Calibrated parameters for the CGMY model: Greece (GR)

B.1.2 Root mean square error (RMSE)

This section presents statistics of the root mean square distributions discussed in Chapter 5. Table B.1 displays the data underlying Figure 5.4.

RMSE	*Sovereign*	*Minimum*	*1st Quartile*	*Median*	*3rd Quartile*	*Maximum*	*Mean*	*Standard Deviation*
Absolute	PT	0.07	1.30	2.74	5.12	64.61	4.72	6.84
	IE	0.09	1.10	1.71	3.15	16.60	2.86	3.18
	IT	0.07	0.82	1.69	2.44	27.24	2.04	2.50
	GR	1.58	10.43	29.10	130.31	13 497.81	413.96	1 434.86
	SP	0.07	1.15	1.96	3.39	10.89	2.38	1.64
Relative	PT	0.02%	0.35%	0.60%	1.20%	5.11%	0.94%	0.99%
	IE	0.04%	0.52%	1.03%	1.52%	3.08%	1.11%	0.73%
	IT	0.02%	0.29%	0.63%	0.97%	5.22%	0.71%	0.68%
	GR	0.37%	2.06%	3.21%	12.28%	49.92%	8.95%	11.47%
	SP	0.02%	0.38%	0.66%	1.24%	3.32%	0.90%	0.74%

Table B.1: Calibration of the CGMY model: descriptive statistics of the optimal root mean square errors (RMSE), for the dataset of weekly CDS spreads with maturities $T \in \{1, 3, 5, 7, 10\}$ years, spanning January 2010 to February 2014.

B.1.3 Default probability term structure

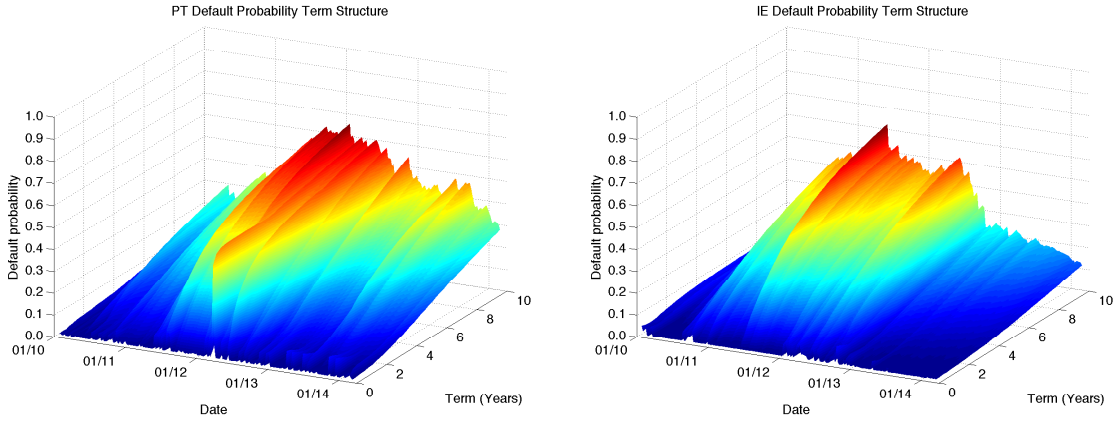

Figure B.6: Default probability term structure: PT and IE sovereigns

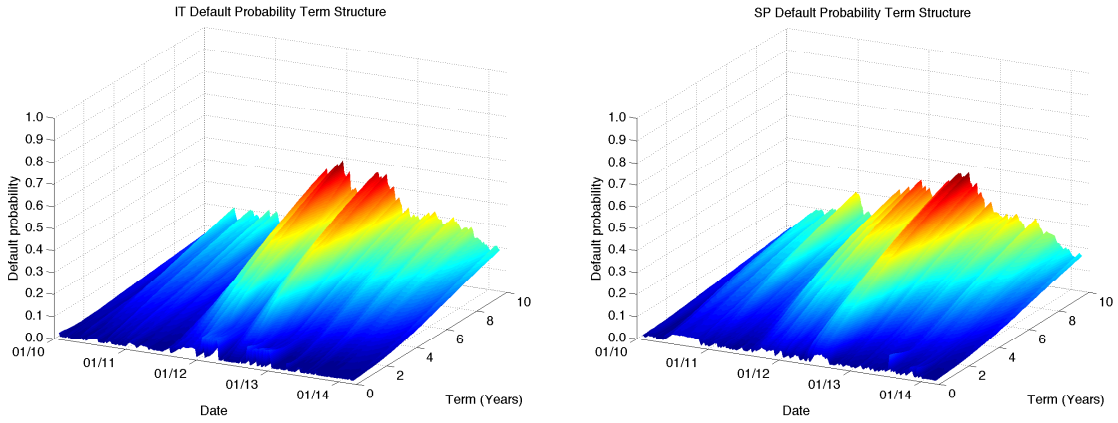

Figure B.7: Default probability term structure: IT and SP sovereigns

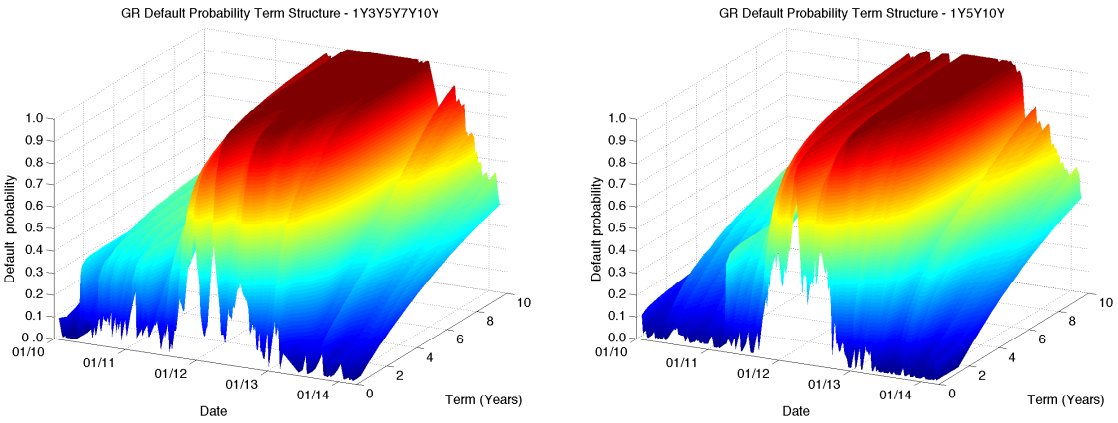

Figure B.8: Default probability term structure: GR sovereign

B.1.4 A comparison with the Brownian motion dynamics

This section provides an empirical illustration of the shortcomings of the geometric Brownian motion dynamics for X_t, when compared to the Lévy dynamics introduced by the CGMY model.

Figure B.9 and Table B.2 present the calibration results for an arbitrarily chosen reference date (2014-02-26). The recovery rate parameter is again set at $R = 0.3$. On the left, the calibrated CDS spreads for both models are plotted against the market data; on the right, the survival functions are compared.

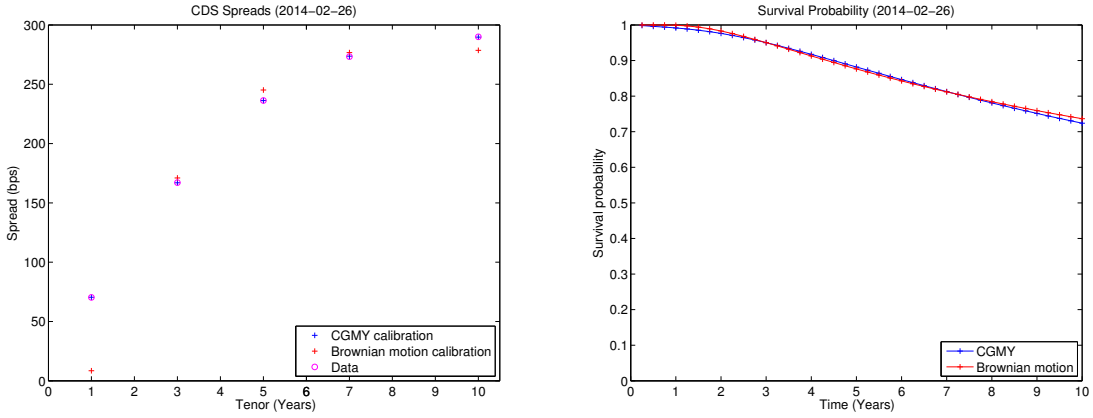

Figure B.9: Comparison of calibrated exponential CGMY and geometric Brownian motion dynamics, for reference date 2014-02-26: CDS spreads and survival probabilities.

Model	*Parameter*	*Calibration*	*RMSE*
Exponential CGMY	C	0.0132	1.32
	G	0.0095	
	M	0.1679	
	Y	0.2035	
Geometric Brownian motion	μ	0.0118	28.49
	σ	0.3718	

Table B.2: Comparison of calibrated exponential CGMY and geometric Brownian motion dynamics, for reference date 2014-02-26: calibration parameters and optimal root mean square error (RMSE). The calibrated CGMY model has negative skewness (as $G > M$), infinite activity and infinite variation (as $1 < Y < 2$). The Brownian motion has continuous sample paths and infinite variation.

The root mean square error is once more used to gauge the accuracy of each model's fit to the data. We can see that the geometric Brownian motion underperforms severely against the exponential CMGY model, failing to adequately capture the CDS spreads behavior, especially for the 1 year, short term tenor. Even though the CGMY model has two extra parameters, we can ascribe this fact to the fundamental difference in the dynamics of both processes.

As compared with the CGMY model, the Brownian motion has higher survival probabilities both for the short and long terms, leading to lower than expected CDS spreads for

these periods (and also higher for intermediate tenors).

These empirical observations reflect the local predictability of defaults under the Brownian motion model and are consistent with the remarks made in Chapter 2.

Table B.3 presents key statistics of the distribution of the absolute and relative RMSEs, for a weekly calibration spanning January to February 2014.

Model	*RMSE*	*Minimum*	*1st Quartile*	*Median*	*3rd Quartile*	*Maximum*	*Mean*	*Standard Deviation*
Exponential CGMY	Absolute	0.20	0.80	1.08	1.70	2.41	1.22	0.72
	Relative	0.10%	0.34%	0.44%	0.70%	1.04%	0.51%	0.30%
Geometric BM	Absolute	28.49	34.81	36.76	39.81	40.54	36.48	4.01
	Relative	13.74%	15.16%	15.54%	15.93%	16.33%	15.41%	0.79%

Table B.3: Calibration of the exponential CGMY vs. geometric Brownian motion models: descriptive statistics of the optimal root mean square errors (RMSE), for the dataset of weekly CDS spreads spanning January 2014 to February 2014.

B.1.5 Transition density

Although the transition density approximation formula (3.1) is crucially employed in the computation of the survival probability, we did not need to use it directly. However, as an illustration, we now provide an example of numerically computed transition densities for the CGMY process in Figure B.10.

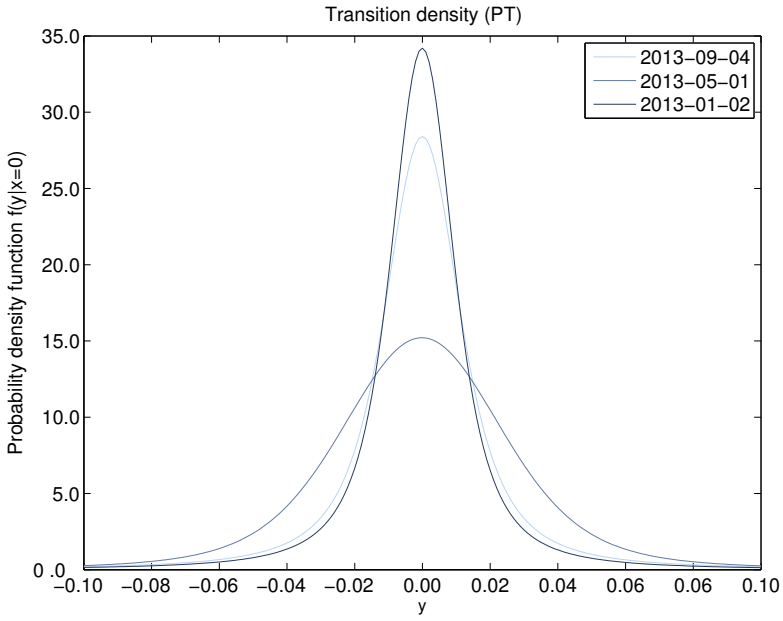

Figure B.10: Numerical estimation of the CGMY transition density for sovereign PT. Three arbitrary dates in 2013 were chosen.

B.2 Multivariate Variance Gamma calibration

B.2.1 Parameters

This section presents the multivariate Variance Gamma (VG) calibration results, for the reference date 2014-02-26. As previously discussed in Sections 6.1.1 and 6.1.2, several calibration scenarios were considered.

Scenarios $i = 1, \ldots, 5$ (marked with 'M', from 'Marginal') denote univariate VG calibrations, for each sovereign $i \in \{\text{PT}, \text{IE}, \text{IT}, \text{GR}, \text{SP}\}$. The optimal parameters $(\sigma_i, \nu_i, \theta_i)$ are obtained by applying the COS method to the VG characteristic function (2.5).

In scenario $i = 6$, we perform the joint, common Gamma time change calibration for all sovereigns. The optimal parameters $(\sigma_i, \nu, \theta_i)$ are also obtained using (2.5), with a single, fixed $\nu_i \equiv \nu$. The following scenario ($i = 7$) restricts the joint calibration to the set of sovereign $\mathcal{S}_C = \{\text{IE}, \text{IT}, \text{SP}\}$. The final scenario ($i = 8$) extends the previous one. Sovereigns $i \in \mathcal{S}_I = \{\text{PT}, \text{GR}\}$ are calibrated conditionally on the common time change component ν. Parameters $(\sigma_i, \theta_i, \alpha_i)$ are computed from the COS method, using (6.5). In scenarios 6–8, the sovereigns marked with 'C' (from 'Common') are calibrated with a joint, common Gamma time change of the form (6.1); the sovereigns marked with 'I' (from 'Idiosyncratic') are calibrated with the addition of an idiosyncratic Gamma time change component, following (6.3).

Calibration Scenario						*Calibration Results*																			
i	*Sovereign*					RMSE		Common Parameter	Idiosyncratic Parameters (PT)				Idiosyncratic Parameters (IE)				Idiosyncratic Parameters (IT)				Idiosyncratic Parameters (GR)				Idiosyncratic Parameters (SP)			
	PT	IE	IT	GR	SP	Absolute	Relative	ν	σ_i	ν_i	ϑ_i	α_i	σ_i	ν_i	ϑ_i	α_i	σ_i	ν_i	ϑ_i	α_i	σ_i	ν_i	ϑ_i	α_i	σ_i	ν_i	ϑ_i	α_i
1	M	-	-	-	-	4.05	1.95%	-	0.35	1.41	-0.03	-			-				-				-				-	
2	-	M	-	-	-	6.65	7.85%	-			-		0.31	2.48	0.03	-			-				-				-	
3	-	-	M	-	-	6.03	4.35%	-			-				-		0.25	2.67	-0.04	-			-				-	
4	-	-	-	M	-	6.38	1.28%	-			-				-				-		1.12	5.77	0.14	-			-	
5	-	-	-	-	M	7.10	5.72%	-			-				-				-				-		0.36	2.82	0.02	-
6	C	C	C	C	C	20.46	9.72%	5.83	0.44	-	-0.01	1.00	0.32	-	0.02	1.00	0.31	-	-0.02	1.00	1.12	-	0.14	1.00	0.40	-	0.03	1.00
7	-	C	C	-	C	5.08	4.39%	2.57			-		0.27	-	0.00	1.00	0.27	-	-0.03	1.00			-		0.36	-	0.02	1.00
8	**I**	**C**	**C**	**I**	**C**	**10.28**	**4.89%**	**2.57**	**0.35**	**0.81**	**-0.02**	**0.68**	**0.27**	**-**	**0.00**	**1.00**	**0.27**	**-**	**-0.03**	**1.00**	**0.83**	**3.99**	**0.14**	**0.68**	**0.36**	**-**	**0.02**	**1.00**

Table B.4: Calibration scenarios and results for reference date 2014-02-26.

Comparing the marginal calibrations (scenarios 1–5) with scenario 6, we see that the common time change parameter ν is significantly higher that the marginal parameters ν_i, for all sovereigns except GR. The calibration of scenario 8 is achieved with the same sensitivity of the time change $H_t^{(i)}$ to the common Gamma component G_t for both sovereigns (PT and GR), namely $\alpha_i \simeq 0.68$.

B.2.2 Joint and conditional default probabilities

This section presents the estimated joint and conditional default probabilities under the multivariate VG model, using the observed CDS spreads at 2014-02-26. For comparison purposes, marginal default probabilities are also provided.

Time Period	*Marginal Default Probability*		*Joint Default Probability*				
			PT	IE	IT	GR	SP
1 Year	PT	0.69%	*NA*	0.02%	0.06%	0.13%	0.04%
	IE	0.27%	0.02%	*NA*	0.02%	0.05%	0.02%
	IT	0.50%	0.06%	0.02%	*NA*	0.08%	0.04%
	GR	5.07%	0.13%	0.05%	0.08%	*NA*	0.12%
	SP	0.63%	0.04%	0.02%	0.04%	0.12%	*NA*
5 Years	PT	11.25%	*NA*	0.73%	1.36%	3.09%	1.17%
	IE	3.74%	0.73%	*NA*	0.63%	1.12%	0.52%
	IT	6.76%	1.36%	0.63%	*NA*	1.99%	0.90%
	GR	24.69%	3.09%	1.12%	1.99%	*NA*	1.86%
	SP	6.32%	1.17%	0.52%	0.90%	1.86%	*NA*
10 Years	PT	27.46%	*NA*	3.62%	6.33%	9.90%	4.66%
	IE	11.13%	3.62%	*NA*	3.02%	4.09%	2.17%
	IT	19.58%	6.33%	3.02%	*NA*	7.22%	3.76%
	GR	35.31%	9.90%	4.09%	7.22%	*NA*	5.52%
	SP	14.84%	4.66%	2.17%	3.76%	5.52%	*NA*

Scale	3%	6%	9%	12%	15%	18%	21%	24%	27%	30%	33%	36%	39%	42%

Table B.5: Joint default probabilities, estimated from a sample of 100 000 jointly simulated paths. Entry (i, j) for time period T represents the estimated joint default probability of sovereigns i and j, $i, j \in \{\text{PT}, \text{IE}, \text{IT}, \text{GR}, \text{SP}\}$, up to time T.

Time Period	*Marginal Default Probability*		*Conditional Default Probability*				
			PT	IE	IT	GR	SP
1 Year	PT	0.69%	*NA*	8.68%	11.55%	2.57%	6.80%
	IE	0.27%	3.34%	*NA*	3.39%	0.97%	3.48%
	IT	0.50%	8.42%	6.42%	*NA*	1.62%	6.33%
	GR	5.07%	18.87%	18.49%	16.33%	*NA*	18.51%
	SP	0.63%	6.24%	8.30%	7.97%	2.31%	*NA*
5 Years	PT	11.25%	*NA*	19.60%	20.12%	12.50%	18.54%
	IE	3.74%	6.52%	*NA*	9.32%	4.52%	8.20%
	IT	6.76%	12.10%	16.83%	*NA*	8.05%	14.25%
	GR	24.69%	27.44%	29.81%	29.40%	*NA*	29.46%
	SP	6.32%	10.41%	13.84%	13.31%	7.54%	*NA*
10 Years	PT	27.46%	*NA*	32.50%	32.33%	28.03%	31.42%
	IE	11.13%	13.17%	*NA*	15.44%	11.58%	14.60%
	IT	19.58%	23.05%	27.17%	*NA*	20.44%	25.35%
	GR	35.31%	36.04%	36.73%	36.86%	*NA*	37.18%
	SP	14.84%	16.98%	19.47%	19.22%	15.63%	*NA*

Scale	3%	6%	9%	12%	15%	18%	21%	24%	27%	30%	33%	36%	39%	42%

Table B.6: Conditional default probabilities, estimated from a sample of 100 000 jointly simulated paths. Entry (i, j) for time period T represents the estimated conditional default probability of sovereign i given the default of sovereign j (both up to time T). The results clearly show dependency between defaults. We can also see that sovereigns PT and IT are more sensitive to the default of other sovereigns, and notice an increase in this sensitivity when T decreases.

Appendix C

Simulating the Variance Gamma process

This section describes the procedure we have followed to simulate the Variance Gamma (VG) process as a Gamma time-changed Brownian motion (TCBM). The univariate simulation is built from the TCBM formula (2.4). For the multivariate VG model, we use (6.4).

We start by defining a time span $[0, T]$ for the simulation of paths, and a time increment $\Delta t := \frac{T}{N}$, where N is the number of discretization steps.

C.1 Univariate simulation

Set $X_0 = 0$. For each $k = 1, \ldots, N$, perform the following steps:

Step 1 Take independent draws ΔG_k and Z_k from the random variables $G \sim \Gamma\left(\Delta t \cdot \frac{1}{\nu}, \frac{1}{\nu}\right)$ and $Z \sim \mathcal{N}(0, 1)$, respectively (independently of the previous step $k - 1$).

Step 2 For $t_k = k \cdot \Delta t$, compute

$$X_{t_k} = X_{t_{k-1}} + \theta \Delta G_k + \sigma \sqrt{\Delta G_k} Z_k.$$

C.2 Multivariate simulation

Set $X_0^{(i)} = 0$ for all sovereigns i. For each $k = 1, \ldots, N$ and each sovereign i, perform the following steps:

Step 1 Take independent draws ΔG_k and Z_k from the random variables $G \sim \Gamma\left(\Delta t \cdot \frac{1}{\nu}, \frac{1}{\nu}\right)$ and $Z \sim \mathcal{N}(0, 1)$, respectively (independently of the previous step $k - 1$). For each sovereign i such that $\alpha_i \neq 1$ (i.e., such that it has an idiosyncratic time change component), take an additional independent random draw $\Delta G_k^{(i)}$ from the idiosyncratic time change component $G^{(i)} \sim \Gamma\left(\Delta t \cdot \frac{1}{\nu_i}, \frac{1}{\nu_i}\right)$;

Step 2 For $t_k = k \cdot \Delta t$, compute the time change increment

$$\Delta H_k^{(i)} = \begin{cases} \Delta G_k & , \alpha_i = 1 \\ \alpha_i \Delta G_k + (1 - \alpha_i) \Delta G_k^{(i)} & , \alpha_1 \neq 1 \end{cases}$$

and the marginal process value:

$$X_{t_k}^{(i)} = X_{t_{k-1}}^{(i)} + \theta_i \Delta H_k^{(i)} + \sigma_i \sqrt{\Delta H_k^{(i)}} Z_k.$$

Bibliography

[1] Almendral A. and Oosterlee C. W. (2007). On American options under the Variance Gamma process. *Appl. Math. Finance 14(2)*, 131-152.

[2] Ané T. and Geman H. (2000). Order flow, transaction clock, and normality of asset returns. *The Journal of Finance, 55(5)*, 2259-2284.

[3] Barndorff-Nielsen O. E. (1977). Exponentially decreasing distributions for the logarithm of particle size. *Proc. Roy. Soc. London Ser. A 353*, 401–19.

[4] Barndorff-Nielsen O. E. (1997). Normal inverse Gaussian distributions and stochastic volatility modelling. *Scand. J. Statis. 24*, 1–13.

[5] Barndorff-Nielsen O. E. (1998). Processes of normal inverse Gaussian type. *Finance Stochast. 2*, 41–68.

[6] Barndorff-Nielsen o. E. and Shephard N. (2001). Non-Gaussian Ornstein–Uhlenbeck based models and some of their uses in financial economics. *J. R. Statis. Soc. B 63*, 167–241.

[7] Black, F. and Cox, J. C. (1976). Valuing corporate securities: Some effects of bond indenture provisions. *The Journal of Finance 31(2)*, 351–367.

[8] Calvo G. A. (1988). Servicing the public debt: The role of expectations. *American Economic Review 78(4)*, 647–661.

[9] Cariboni J. and Schoutens W. (2008). Pricing credit default swaps under Lévy models. *Journal of Computational Finance 10(4)*, 71-91.

[10] Cariboni J. and Schoutens W. (2009). *Lévy processes in credit risk*. Wiley Finance.

[11] Carr P., Chang E. C. and Madan D.B. (1998). The variance gamma process and option pricing. *Eur. Finan. Rev. 2*, 79–105.

[12] Carr P., Geman H., Madan D. B., Yor M. (2002). The fine structure of asset returns: an empirical investigation. *J. Business 75*, 305–33.

[13] Clark P. (1973). A Subordinated Stochastic Process Model with Fixed Variance for Speculative Prices. *Econometrica, 41*, 135-156.

[14] Clark E. and Kassimatis K (2004). Country financial risk and stock market performance: the case of Latin America. *Journal of Economics and Business 56*, 21-41.

[15] Cont R. and Tankov P. (2004). *Financial Modeling with Jump Processes*. Chapman & Hall/CRC, Boca Raton, FL.

[16] Currie E. and Velandia A. (2002). Risk management of contingent liabilities within a sovereign asset-liability framework. World Bank Working Paper.

[17] Eaton J. and Gersovitz M. (1981). Debt with Potential Repudiation: Theoretical and Empirical Analysis. *The Review of Economic Studies 48*, 289-309.

[18] Fang F., Jönsson H., Oosterlee C. W. and Schoutens W. (2010). Fast Valuation and Calibration of Credit Default Swaps Under Lévy Dynamics. *Journal of Computational Finance 14(2)*, 57-86.

[19] Fang F. and Oosterlee C. W. (2009). Pricing Early-Exercise and Discrete Barrier Options by Fourier-Cosine Series Expansions. *Numerische Mathematik 114*, 27-62.

[20] Fang F. and Oosterlee C. W. (2008). A novel option pricing method based on Fourier-cosine series expansions. *SIAM J. Sci. Comput. 31(2)*, 826-848.

[21] Hui C. H. and Lo C. F. (2002). Valuation Model of Defaultable Bond Values in Emerging Markets. *Asia-Pacific Financial Markets 9*, 45-60.

[22] Hurd T. R (2009). Credit Risk Modelling using Time-Changed Brownian Motion. *International Journal of Theoretical and Applied Finance Vol. 12 No. 8*, 1213–1230.

[23] Hurd T. R. and Kuznetsov A. (2009). On the first passage time for Brownian motion subordinated by a Lévy process. *Journal of Applied Probability 46.1*, 81-198.

[24] Hurd T. R. and Zhou Z. (2011). Structural credit risk using time-changed Brownian motions: a tale of two models. Working paper.

[25] Karmann A. and Maltritz D. (2003). Sovereign Risk in a Structural Approach. Evaluating Sovereign Ability-to-Pay and Probability of Default in: Bol, G. *et al.* (Ed.), *Credit Risk - Measurement, Evaluation and Management.* Heidelberg / New York, 91-109.

[26] Kou S. G. (2002). First passage time of a jump diffusion process. *Advances in Applied Probability 35*, 504–531.

[27] Kou S. G., Petrella G. and Wang H. (2005). Pricing path-dependent options with jump risk via Laplace transforms. *Kyoto Economic Review 74*, 1–23.

[28] Kou S. G. (2007). Jump-Diffusion Models for Asset Pricing in Financial Engineering. *Handbooks in Operations Research and Management Science: Financial Engineering Volume 15*, Elsevier Science.

[29] Lando D. (2004). *Credit Risk Modeling, Theory and Applications.* Princeton University Press, 2004.

[30] Madan D. and Seneta E. (1990). The variance gamma (V. G.) model for share market returns. *J. Business 63*, 511–524.

[31] Madan D. and Yor M. (2008). Representing the CGMY and Meixner Lévy processes as time-changed Brownian motions. *Journal of Computational Finance 12(1)*, 27-47.

[32] Mandelbrot B. (1963). The variation of certain speculative prices. *J. Busin. 36*, 394–419.

[33] Merton R. (1974). On the Pricing of Corporate Debt: The Risk Structure of Interest Rates. *Journal of Finance 29(2)*, 449–470.

[34] Merton R. (1976) Option pricing when underlying stock returns are discontinuous, *J. Financial Econ. 3*, 125–44.

[35] Monroe I. (1978). Processes that can be embedded in Brownian motion. *Ann. Prob. 6*, 42–56.

[36] Moody's Investors Service (2014). Sovereign Default and Recovery Rates, 1983–2013.

[37] Moreira A. and Rocha K. (2004). Two-Factor Structural Model of Determinants of Brazilian Sovereign Risk. *The Journal of Fixed Income 14*, 48-59.

[38] Oshiro N. and Saruwatari Y. (2005). Quantification of sovereign risk: Using the information in equity market prices. *Emerging Markets Review 6*, 346-362.

[39] Papapantoleon, A. (2008). An introduction to Lévy processes with applications in finance. Lecture notes, TU Vienna, available at http://page.math.tu-berlin.de/papapan/publications.html.

[40] Rogers L. C. G. (1997). Arbitrage with fraction Brownian motion. *Math. Finance 7*, 95-105.

[41] Sato K. (1999). *Lévy Processes and Infinitely Divisible Distributions.* Cambridge University Press, Cambridge.

[42] Schönbucher P. J. (2003). *Credit Derivatives Pricing Models: Models, Pricing and Implementation.* Wiley Finance.